ERASMUS MUNDUS MSC PROGRAMME

COASTAL AND MARINE ENGINEERING AND MANAGEMENT
COMEM

CLIMATE CHANGE IMPACTS ON MIXING AND CIRCULATION AT SONGKHLA LAGOON, THAILAND

TU Delft
June 2011

Bruno Vicente Primo de Siqueira
4055241


Education and Culture DG


CoMEM

The Erasmus Mundus MSc Coastal and Marine Engineering and Management is an integrated programme organized by five European partner institutions, coordinated by Delft University of Technology (TU Delft).
The joint study programme of 120 ECTS credits (two years full-time) has been obtained at three of the five CoMEM partner institutions:

- Norges Teknisk- Naturvitenskapelige Universitet (NTNU) Trondheim, Norway
- Technische Universiteit (TU) Delft, The Netherlands
- City University London, Great Britain
- Universitat Politècnica de Catalunya (UPC), Barcelona, Spain
- University of Southampton, Southampton, Great Britain

The first year consists of the first and second semesters of 30 ECTS each, spent at
NTNU, Trondheim and Delft University of Technology respectively.
The second year allows for specialization in three subjects and during the third semester courses are taken with a focus on advanced topics in the selected area of specialization:

- Engineering
- Management
- Environment

In the fourth and final semester an MSc project and thesis have to be completed.
The two year CoMEM programme leads to three officially recognized MSc diploma certificates. These will be issued by the three universities which have been attended by the student. The transcripts issued with the MSc Diploma Certificate of each university include grades/marks for each subject. A complete overview of subjects and ECTS credits is included in the Diploma Supplement, as received from the CoMEM coordinating university, Delft University of Technology (TU Delft).

Information regarding the CoMEM programme can be obtained from the programme coordinator and director

Prof. Dr. Ir. Marcel J.F. Stive
Delft University of Technology
Faculty of Civil Engineering and geosciences
P.O. Box 5048
2600 GA Delft
The Netherlands

Preface

This report forms my Master of Science thesis and is the completion of my study of CoMEM (Coastal and Marine Engineering and Management) at the faculty of Civil Engineering and Geosciences at the Delft University of Technology.

This study is part of a project called "Climate Change Impacts on Small Tidal Inlets (CC-STI)" lead by UNESCO-IHE.

The committee of this MSc thesis consisted of the following persons:

Prof.dr.ir. M.J.F. Stive (Chairman, Delft University of Technology)

Dr. R.W.M.R.J.B. Ranasinghe (Delft University of Technology/UNESCO-IHE)

Ir. D.J.R. Walstra (Delft University of Technology/Deltares)

Dr. N. Geleynse (Delft University of Technology)

Bruno Vicente Primo de Siqueira

June, 2011

Acknowledgments

I would like to thanks the Erasmus Mundus program for giving the opportunity to provide me a high quality master in the best universities of Europe and the possibility to meet people from different nationalities. In particular, I would like to thank them for granting me my scholarship, which made this MSc possible.

I would like to thank this MSc thesis committee for their patience and attention towards me. Especially to my advisor and friend Dr. Rosh Ranasinghe for sharing knowledge and support during the whole process.

I would also like to thank Dr. Sutat Weesakul of AIT for providing all field data, Dr. Sarith Mahanama of NASA, Washington DC for all riverflow projections and Arjen Luijendijk for his help at the initial stages.

I would like to thank Fernanda Achete for all the help, patience, for listening, for being there and to take care of me.

Summary

Coastal lagoons are shallow coastal water bodies separated from the ocean by a barrier and they support a range of natural services that are highly valued by society, including but not limited to fisheries productivity, storm protection, and tourism. Songkhla lagoon is the largest lagoonal water resource in Thailand and Southeast Asia. The lagoon is a combined freshwater and estuarine complex of high productivity which represents an extraordinary combination of environmental resources believed to be unique in the region.

Climate change, as a response to increased greenhouse gases in the Earth's atmosphere, is now a widely accepted phenomenon. Sea level rise, temperature, precipitation, and storminess are expected to change significantly with global climate change and to impact coastal lagoons. The nature and magnitude of these impacts are still not very clear. The general objective of the research is to determine the climate change impacts on mixing and circulation at Songkhla lagoon, Thailand.

To achieve this objective the lagoon was be modeled with Delft 3D, a model developed by Deltares. After the verification with the available data for the region, different scenarios were created to represent the possible changes in mean sea level and riverflow due to global warming. Then, these results were compared to the current conditions to determine the main changes in mixing and circulation in this coastal lagoon.

The results suggest an increase in water velocities of the inlet in future scenarios and a decrease of flushing time. Salinity and stratification showed more complex changes in futures scenarios.

Contents

List of Figures

List of Tables

List of Symbols

Symbol	Description
u	flow velocity in the ξ direction
v	flow velocity in the η direction
ω	flow velocity in the z direction
f	Coriolis parameter
P_η	Gradient hydrostatic pressure in the η direction
P_ξ	Gradient hydrostatic pressure in the ξ direction
F_η	Turbulent momentum flux in the η direction
F_ξ	Turbulent momentum flux in the ξ direction
M_η	Source of sink of momentum in the η direction
M_ξ	Source of sink of momentum in the ξ direction
R	Earth radius
λ	Latitude
ϕ	Longitude
ζ	Water level above a reference plan
d	Depth below a horizontal reference plane
Q	Contributions per unit area due to the discharge or withdrawal of water
H	Total water depth
ν_V	Vertical eddy viscosity
w	Fluid velocity
$\sqrt{G_{\xi\xi}}$	Coeficient used to transform curvilinear to rectangular co-ordinates
$\sqrt{G_{\eta\eta}}$	Coeficient used to transform curvilinear to rectangular co-ordinates

1. Introduction

1.1. General

Coastal lagoons are recognized as one of the most sensitive types of estuaries to human intervention due to the dynamic nature of their entrances, and general lack of tidal flushing. The environmental processes of coastal lagoons are largely driven by the condition of the inlet. Meanwhile, entrance behavior is driven by the dynamic balance between oceanic processes such as tides, waves and mean sea level (MSL), and fluvial/estuarine processes such as stream flow and heat fluxes. Small Tidal Inlets (STIs) are common in tropical and sub-tropical developing countries and particularly in monsoonal environments.

This study is part of a project called "Climate Change Impacts on Small Tidal Inlets (CC-STI)" lead by UNESCO-IHE. For the purposes of this study, small tidal inlets are defined as those with inlet channels that are less than 500m wide, and are connected to estuaries/lagoons with surface areas less than 50 km2. Such inlets are common in tropical and sub-tropical regions (e.g. India, Sri Lanka, Vietnam, Florida (USA), and South America (Brazil), South Africa, and SW/SE Australia). The main objective of CC-STI is to determine how the climate change will impact on STIs and what the best adaptation strategies are. To achieve this aim, one of the steps of the project, which this study is included, is to determine the climate change impacts on water quality, mixing and circulation characteristics in STIs along the SW coast of the Gulf of Thailand.

Songkhla lagoon is the largest lagoonal water resource in Thailand and Southeast Asia and is made up of three interconnected lakes. Southern Songkhla Lake, known as Thale Sap Songkhla, is the outer lagoon of the system and empities into the Gulf of Thailand through a small channel which also serves as the harbor entrance to the town of Songkhla.

The depth of the harbor and its channel are maintained at six to eight meters. An open lagoon with an undisturbed circulation of fresh and brackish water is a prerequisite for a stable and healthy ecosystem. Any change in this dynamic, whether from natural or man-induced actions, is likely to affect the whole system.

Future climate change (CC) is expected to change both rainfall and coastal processes. Climate change therefore will lead to potentially wide ranging changes to coastal lagoon environments (including physical, chemical and ecological processes). These impacts are likely to result in significant socio-economic, environmental and ecological losses.

Using downscaling global atmospheric ocean circulation models (ECHAM and GFDL) to predict local future hydrological behavior and IPCC projections to determine future sea level rise, some scenarios were created. These scenarios were modeled, using a validated process based 3D model (Delft3D) and the results compared with the present situation to determine the potential CC impacts on circulation and mixing.

1.2. Objectives of Study

The general objective of this study is to determine the climate change impacts on mixing and circulation at Songkhla lagoon, Thailand.

The specific objectives of the research are:

- Analyze the available data of water level, velocity, salinity and streamflow of Songkhla Lagoon.
- Model the area using Delft 3D and determine the present situation of the lagoon in terms of circulation and mixing.
- Create future scenarios of hydrological behavior and sea level rise for the area based on dynamically downscaled Global Circulation Model output.
- Determine the impacts of the different future CC modified scenarios on mixing and circulation of Songkhla lagoon.

2. Literature Review

2.1. Coastal lagoons

2.1.1 General

A coastal lagoon is a shallow water body separated from the ocean by a barrier, connected at least intermittently to the ocean by one or more restricted inlets, and usually oriented shore-parallel (Kjerfve, 1994). They account for thirteen percent of all coastal environments and usually are poorly flushed and exhibit long resident times (Barnes, 1980).

From an evolutionary point of view, coastal lagoons are ephemeral on a geologic time scale and were formed by a combination of longshore drift and sea-level variation (Kjerfve, 1994). The sea level rose 130m near the end of Pleistocene (15000 years ago) and flooded river valleys and low-lying coastal depressions. Usually, the sediment transport processes caused the reshape of the coast, such as growing of spits and barriers and formed the lagoons (Kjerfve, 1989). However, there are also some cases where coastal lagoons were formed in marginal depressions behind barriers of reworked deltaic sediments (Nichols and Allen, 1981) in active river delta systems. Such lagoons are often oriented normal to the coast, instead of parallel, for instance, Lake Calcasieu, Lousiana, and Lagoa Feira, Brazil. (Kjerfve, 1989)

Coastal lagoons are formed and maintained through sediment transport processes (Anthony, 2009). They are often subject to rapid sedimentation, and will eventually change into other types of environments through sediment infillting, tectonic activity, eustatic change in sea level, and land-use activities. This change is geogically rapid and can be expected to occur within decades to centuries (Kjerfve, 1989).

The size of coastal lagoons varies substantially, ranging in area from less than 0.01km2 to more than 10000 km2, as in the case of Lagoa dos Patos in Brazil. The depth is often 1-3m and rarely is more than 5m except for the inlet and other channels. Salinity also can vary substantially, depending on local climatic conditions, lagoons can exhibit salinity that range from completely fresh to hypersaline. (Kjerfve, 1994).

Coastal lagoons support a range of natural services that are highly valued by society, including but not limited to fisheries productivity, storm protection, and tourism. They are highly productive ecosystems and contribute to the overall productivity of coastal waters by supporting a variety of habitats including salt marshes, seagrasses, and mangroves. They also provide essential habitat for many fish and shellfish species. (Anthony, 2009)

Coastal lagoons experience the same force functions as coastal plain estuaries: river input, wind stress, tides, precipitation to evaporation balance, and surface heat balance. However, they respond unequally to these forcing functions because of differences in geomorphology. Water and salt balances, lagoon water quality, and eutrophication depends critically on lagoon circulation, salt and material dispersion, water exchange through the ocean canals, and turnover, residence, or flushing times (Kjerfve, 1994).

Whereas circulation, mixing and exchange have been studied extensively in coastal plain estuaries, these processes have been less synthesized for coastal lagoons. However, the dependence of water quality and eutrophication on flushing, hydrodynamic turnover and physical dynamics is of prime importance for planning and implementation of coastal management strategies in coastal lagoons (Kjerfve, 1989).

According to water exchange with the ocean, coastal lagoons can be sub-divided into three geomorphic types (Figure 1). The rate and magnitude of oceanic exchange reflects both the dominant forcing function and the time scale of hydrologic variability (Kjerfve, 1986).

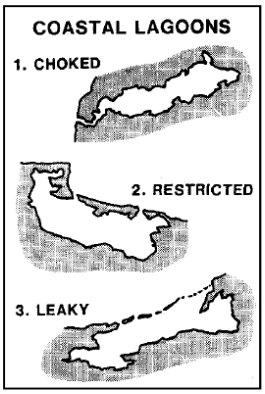

Figure 1 - Coastal lagoons can be conveniently subdivided into choked, restricted and leaky systems based on the degree of water exchange with the adjacent coastal ocean (Kjerfve, 1986).

Choked lagoons are characterized by a single narrow entrance channel, long flushing times, dominant wind forcing, and intermittent stratification events. Usually found along coasts with high wave energy and significant littoral drift, the entrance channel acts as a dynamic filter which largely eliminates tides inside the lagoon. Restricted lagoons usually exhibit two or more entrance channels or inlets, have a well-defined tidal circulation, are influenced by winds, and are usually vertically mixed. Leaky lagoons are enlongated shore-parallel water bodies with many ocean entrance channels. Usually found along coasts where tidal currents are sufficiently strong to overcome the tendencies by littoral drift to close the channels entrances (Kjerfve, 1986).

2.1.2 Water balance

The hydrologic equation is an equation of continuity that explains volume changes in terms of processes that involve both salt water and fresh water:

$$\frac{\Delta V}{\Delta t} = P - E + D + G + A$$

Where V is the volume of the lagoon, P and E are the spatially integrated precipitation and evaporation rates, D is the freshwater discharge, G is groundwater seepage and A is the advective gain or loss of water through a transverse cross-section. All terms are commonly expressed in units of m3/s.

The terms of the equation have considerable temporal variability. Precipitation, Evaporation and Freshwater discharge show variations over time scales ranging from days to seasons. Shallow water are highly responsive to temporal variations to tidal and wind forcing, thus, the advective movement of water is the most rapidly fluctuating term (Miller et al. 1990).

Water motions in coastal lagoons occur over many time and space scales (Figure 2). Circulation, mixing and material transport occur as a result of tides, runoff, weather, episodic stoms, wind, density gradients, sea-level oscillations and changes in heat and water balance (Kjerfve and Magill, 1989).

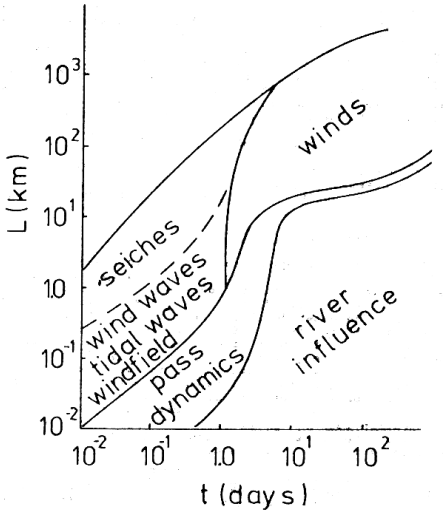

Figure 2 - Relevant time and space scales of forcing in lagoons (Miller et al. 1990)

2.1.3 Circulation

The main geomorphological factors influencing the circulation in a coastal lagoon are the inlet configuration and dimensions, lagoon size and orientation, bottom topography and mean depth. Inlet dimensions control the exchange of water, including dissolved and suspended material. Bottom topography, including natural or artificial channels, plays an important role in guiding the circulation of the lagoon (Smith, 1994).

The circulation within a coastal lagoon can be thought as a response to local and nonlocal, or remote forcing. Local forcing can be sub-divided in two kinds: local wind acting on the surface and creating frictional circulation; and horizontal density gradient due to freshwater entering from the rivers and salt water entering from the inlet. Nonlocal forcing includes tidal, rivers and low-frequency variations in coastal sea level (Miller et al. 1990).

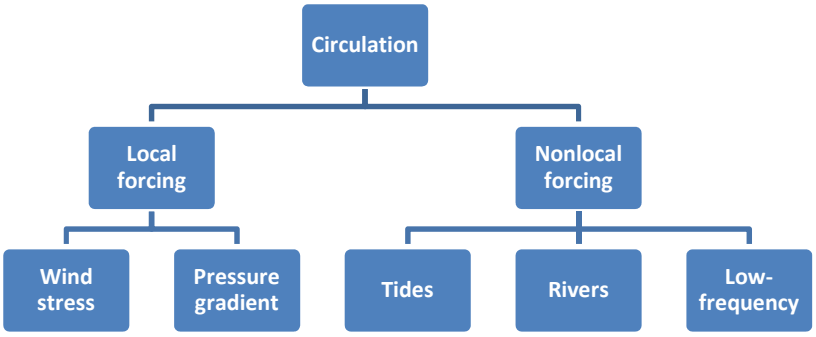

Figure 3 - Forcings of Circulation in a Coastal Lagoon

The various current components that may be superimposed at a particular time and place can be sorted out to some degree when observations in a time series are decomposed into quasi steady, periodic and aperiodic components. For each measument, u, in a time series, we can write:

$$u = \langle u \rangle + U + u' + u''$$

Where $\langle u \rangle$ is the mean over the time period of the study, U is the sinusoidal ebb and flood of the tide, u' is the high frequency non periodic residual and u'' is the low frequency non periodic term, usually associated with wind forcing circulation (Smith, 1994).

2.1.3.1 Wind Stress

The wind-driven component can be considered a local forcing when acts on the lagoon surface and causes frictional circulation. The wind-driven circulation will dominate the nontidal circulation of lagoons with restricted exchanges with ocean. Usually, winds have a seasonal behavior, which will result in corresponding changes in the wind-driven circulation, and thus in the net transport (Miller et al. 1990).

Local forcing by wind produces a direct downwind transport regardless of the wind direction. This will result in a set up water levels along the downwind shore, a set down along the upwind shore and consequently an upwind directed slope in the free surface of the lagoon. This effect will be especially pronounced if the lagoon is elongated in the wind direction. Normally, this set up will not be significant unless the lagoon has a longitudinal axis on the order of several tens of kilometers. The secondary response is an upwind directed return flow. This generally occurs at near-bottom levels and may be aided by navigational channels. This movement can be considered as a response of the pressure gradient forcing (Smith, 1994).

2.1.3.2 Pressure gradient

The pressure is given by

$$p(z) = \int_{\eta}^{z} \rho g dz$$

Where ρ water density and g is is gravity. The water density can vary horizontally and vertically. Furthermore, as described above, the surface of the lagoon is influenced by wind set up and set down, and also by river flow and tides. Therefore, a volume of water, at some intermediate depth z, can experience pressure gradient due to a slope in the free surface, or due to density gradients (Smith, 1994).

$$\alpha \frac{\delta p}{\delta x} = \alpha \frac{\delta(\rho g z)}{\delta x} = \alpha g z \frac{\delta \rho}{\delta x} + g \frac{\delta z}{\delta x}$$

The first term, describes the pressure gradient due to changes in density and it is called baroclinic pressure gradient. Usually the less important term, the baroclinic pressure gradient will always be directed toward regions of lower salinity. Under most circumstances, salinity is a far more important determinant of water density in lagoons and estuaries because temperature differences either across or from top to bottom in a lagoon are small compared to salinity differences. It is important to note that the baroclinic pressure is directly related to depth. Thus, it will increase in importance at bottom layers. The second term is

independent of depth and is related to the tilt of the free surface and is called barotropic pressure gradient. (Miller et al., 1990).

2.1.3.3 Low frequency

The low frequency rise and fall of coastal sea level in response to changes in surface pressure and wind conditions produce an inflow and outflow over time scales on the order of a few days or longer. Remote wind effects are manifested by oscillations in coastal sea level with a period of 2-20 days in response to synoptic wind stress. These effects are more important in restricted and leaky lagoons, where the wind-influenced continental shelf response propagates readily into the system and causes large changes with respect to water level and currents (Kjerfve and Magill, 1989).

The main response to far-field forcing in lagoons is low-frequency coastal water level variations that result in water surface slopes and lagoon water infilling or discharge. During times of infilling, extensive areas bordering the lagoon may become inundated as water level increases (Kjerfve and Magill, 1989).

2.1.3.4 Rivers

Significant river discharges, when they interact with sea water or bracking lagoonal water can result in gravitational (baroclinic) currents inside the lagoon. Usually, the velocity of gravitational currents in lagoons is less than 0.10 m/s, which is considerably smaller than tidal currents in inlets. However, they are still the main cause of water exchange in many systems. Restricted and leaky lagoons show a residual outflow up to 10-40 times larger than the river discharge. (Kjerfve and Magill, 1989).

Gravitational circulation cannot be considered steady or persistent. Gravitational circulation has been found to occur only 43% of the time, with each occurrence generally lasting for no more than five tidal cycles (Kjerfve and Magill, 1989).

2.1.3.5 Tidal Circulation

Tidal currents (a horizontal motion) are a result of the rise and fall of the water level due to tides (a vertical motion). The effects of tidal currents on the movement of water in and out of coastal lagoons can be substantial.

Tidal motions arise in response to forces associated with the interaction of the earth-moon-sun system. The response to this forcing is quantified by individual tidal constituents at approximately semi-diurnal, diurnal, monthly, annual and other periodicities. Each constituent is represented by harmonic constants, amplitudes and phase angles which define the magnitude and time of the rise and fall in water level for

that constituent. Thus, to describe tidal currents in detail, a careful harmonic analysis of the data must be conducted. Ideally, at least a 29-day time series should be available to include a complete lunar synoptic month (Smith, 1994).

The observed tidal current can be represented by:

$$U = \sum_i A_i \sin(\omega_i + \varphi_i)$$

Where A is the amplitude of the ith constituent, ω is its angular frequency and φ is the phase angle.

2.1.3.6 Residual currents

The tidal ebb and flood is the most important feature of the tidal circulation, nevertheless the associated residual flow is especially important as a baseline measure of the circulation. The residual flow results from unequal ebb and flood transport during a complete tidal cycle. This unequally arise from the phase relationship of tidal fluctuation in currents and water level, from nonlinear interactions between the tidal flow and bottom topography, from density gradients, wind stress and from net freshwater discharge (Miller et al., 1990).

According to Van de Kreeke and Cotter (1974) the residual flow is proportional to the ratio of tidal amplitude to water depth. Thus, a significant residual flow requires either a large amplitude tide or shallow water. Usually, coastal lagoons do not have big tides, but they do provide shallow water and thus exhibit residual flow. Residual motion can be divided into two components, one related to the steady flow of water and the other one related to oscillatory motions.

The first is called "Eulerian residual flow" and can be obtained by taken the average of the individual current measurements made over a appropriate time interval such as a tidal period. In mathematical terms, Eulerian residual flow is given by

$$Q_E = \langle u \rangle$$

Where u is the current speed and the brackets indicate a temporal average over a tidal cycle or other appropriate time interval. Eulerian flow quantifies freshwater outflow, all long-period wind driven transport and other nontidal flow in response to lagoon-shelf exchanges onto which tidal oscillations are superimposed.

The second term is called "mass transport Stokes drift" and arises from the correlation of the rise and fall water level with the ebb and flood of the current. The mass transport Stokes drift is given by:

$$Q_s = \frac{\langle \tilde{u}\tilde{H} \rangle}{\langle H \rangle}$$

Where $\tilde{u} = u - \langle u \rangle$ and $\tilde{H} = H - \langle H \rangle$, the differences between the individual measurements and the temporal mean values. A Stokes drift in the direction of tidal wave propagation will arise when over half of the flood tide coincides with water levels above the tidal cycle mean. While Q_s is especially well-suited for describing transport in a co-oscillating current system, the Eulerian residual current generally has to be evaluated as well. In lagoons with both quasi-steady and oscillatory currents, the mass transport residual current $Q_L = Q_E + Q_s$ is calculated to quantify the total transport (Smith, 1994).

In lagoons with a single pass, the Eulerian and Stokes residual motions often transport water in opposite directions.

2.1.3.7 Hydrodynamic exchange with the ocean

Inlet geometry is a very important feature for the circulation inside the lagoon. The pass acts as a filter on the water exchange, which the damping effect is different according to the frequency of water level signal in coastal sea level. Depending on inlet size, tidal amplitudes may be greatly reduced inside the lagoon, while low-frequency variations, may be identical in the lagoon and coastal waters. Semi-diurnal tidal components will also be preferentially damped compared to diurnal components. The total volume of water exchanged increases with the period of the tide for a fixed amplitude tide. The form number, f, is defined by the sum of the amplitudes of the two principal semi-diurnal tidal constituents, divided by the sum of the amplitudes of the principal diurnal constituents:

$$f = \frac{M2 + S2}{K1 + O1}$$

The form number characteristically decreases in magnitude within a coastal lagoon. As noted above, it may be greater than unity in shelf waters, but less than unity inside the lagoon (Smith, 1994).

There are two commonly used measures of lagoon flushing: hydraulic replacement time and freshwater resident time. The hydraulic replacement time is given by

$$T_h = \frac{V}{Q_f}$$

Where V is the mean volume of the lagoon, and Q_f is the total net freshwater discharge. The freshwater replacement time is given by

$$T_f = T_h \frac{(S_0 - S_1)}{S_0}$$

Where S_0 and S_1 are the mean salinities of shelf waters and the lagoon, respectively. Usually, surface runoff is used for Q_f not considering the effects of groundwater seepage, direct precipitation and evaporation. This approximation can lead to substantial over or underestimates in the flushing rate (Smith, 1994).

2.1.4 Mixing

Mixing of water masses with different salinity and temperature characteristics gives rise to density gradients. These gradients drive baroclinic currents as a result of non-parallel isopycnal and isobaric surfaces. Therefore, the density fields will be redistributed by these baroclinic currents. The density and velocity fields are dynamically coupled through a set of non-linear hydrodynamic and mass balance equations (Kjerfve and Magill, 1989).

The interaction between the solar heating, tidal stirring and lagoon circulation give rise to diurnal or semi-diurnal vertical stratification/de-stratification cycle. There are also long period cycles related to seasonally changes of solar heating, wind stirring, estuarine circulation and convective cooling (Ranasinghe and Pattiaratchi, 1999).

The vertical stratification results from the gravity forces moving the densest water to the bottom and with intense mixing, the water column becomes homogeneous. Tidal currents usually with denser water, coupled with river flow with fresh water, results in both vertical and horizontal density stratification. Normally, during periods of quiescence and low freshwater inflow, strong vertical density gradients can be formed in choked and restricted lagoons as a result of surface heat exchange. According to Pritchard (1955), coastal lagoon can be classified in highly stratified, partially mixed and well-mixed according to circulation and stratification characteristics (Kjerfve and Magill, 1989).

2.1.5 Salt Balance

The most basic distinction in salt transport mechanisms is between advective transport and non-advective, diffusive processes. Over time scales longer than several days, at least, lagoons with a sufficiently strong and consistent freshwater outflow will have a quasi steady seaward directed advective transport and a landward directed salinity gradient that drives an upstream diffusion of salt. Over the longest time scales, a balance of these two processes maintains the brackish water conditions in the lagoon. Over shorter time scales, however, meteorological forcing in one form or another can effect significant imbalances,

redistribute salinity within the lagoon and produce significant variations in salinity patterns. Any of the mass transport mechanism noted previously can advect salt as well. Thus, the salt balance of a coastal lagoon is intimately related to the water balance (Smith, 1994).

2.1.6 Flushing

The residence time of water within an estuary, or flushing time, is the most important indicator of water quality in the estuary (Dyer, 1973; Fischer et al., 1979; Sanford et al., 1992; Sheng et al., 1996). To assess the fate and effects of pollutants and nutrients discharged into the estuary, it is essential that the flushing time of the estuary is defined accurately. When the flushing time is large, the pollutants/nutrients remain within the estuary for a long period while when the flushing time is small, the pollutants/nutrients are readily transported out of the estuary. Flushing time is often difficult to estimate through field measurements. Therefore, estimates must be obtained through the use of appropriate models.

The flushing time of an estuary can be governed by tides, wind, or streamflow (Dyer, 1973; Fischer et al., 1979; Sanford et al., 1992). Tidal flushing is produced through repeated exchange of the intertidal volume, or tidal prism, between the estuary and the ocean. Water entering the estuary during the flood phase of the tide fills the intertidal volume until high tide is reached. During the ebb phase of the tide, the intertidal volume of water flows out of the estuary. Models based on the flushing mechanism are known as ‘Tidal Prism Models’ and have been in use for quite some time. A number of 'Tidal Prism Models are described in detail by Dyer (1973) and also by Fischer et al. (1979). However, two major shortcomings of these models are pointed out by Sanford et al. (1992) as: (a) the assumption that al water entering on the flooding tide is fully mixed with ambient estuarine water, and (b) the proportion of flushed water that returns to the estuary on the following flooding tide, or the return flow factor, is assumed to be zero. Sanford et al. (1992) present an improved Tidal Prism Model, where streamflow and the return flow factor are taken into account. However, this model still assumes complete mixing of estuarine water, which is not a realistic assumption.

Wind affects surface velocities and could result in the generation of a circulation pattern as explained in section 2.2.3. This would have a direct effect (negative or positive) on flushing time. The magnitude of the effect would depend on variables such as wind speed, direction, and the duration of the wind event (Fischer et al., 1979; Sanford et al., 1992). Wind is also a primary source of mixing (see section 2.2.2) which has an effect on flushing. For example, if the estuary is strongly stratified streamflow that enter the estuary as a buoyant surface jet would remain on the upper layers and rapidly transport the pollutants/nutrients resident in the streamflow out of the estuary there by reducing the flushing time. Wind events capable of improving flushing are likely to last for several days which is often the critical

period for adequate flushing to maintain good water quality (Sanford et al., 1992). Simple models that take the effect of wind on flushing into account do not exist in the literature. One option to evaluate the effect of wind on flushing is to use a 3-demensional hydrodynamic model.

Riverflow is another process that could affect flushing. The flushing time can be affected in two ways by streamflow. Firstly, significant streamflow can increase the intertidal volume that accumulates within the estuary during the flooding tide, thus reducing the flushing time. This effect of streamflow is incorporated in most Tidal Prism Models (Dyer, 1973; Fischer et al., 1979; Sanford et al., 1992). The second effect is the generation of longitudinal, horizontal, or transverse circulation patterns as described in section 2.2.3. The intensity, net-direction, and duration of these circulation patterns can greatly influence flushing time (Sheng et al., 1996; Smith, 1996). Apart from using a sophisticated 3-D hydrodynamic model, there is no other option to include the full effect of streamflow on flushing (Smith, 1996).

2.2. Climate change

2.2.1 General

Warming of the climate system is unequivocal, as is now evident from observations of increases in global average air and ocean temperatures, widespread melting of snow and ice and rising global average sea level. Impacts of a changing climate are already beginning to emerge (Steffen, 2006).

The energy balance of the climate system is affected by changes in atmospheric concentrations of greenhouse gases (GHGs) and aerosols, land cover and solar radiation. Most of the observed increase in global average temperatures since the mid-20th century is very likely due to the observed increase in anthropogenic GHG concentrations, such as carbon dioxide and methan. It is likely that there has been significant anthropogenic warming over the past 50 years averaged over each continent (IPCC, 2007)

Observational evidence from all continents and most oceans shows that many natural systems are being affected by regional climate changes, particularly temperature increases (IPCC, 2007).

There is high agreement and much evidence that with current climate change mitigation policies and related sustainable development practices, global GHG emissions will continue to grow over the next few decades (IPCC, 2007).

The possible impacts of climate change that might affect coastal lagoons includes: temperature changes, sea level rise, storms more frequent and stronger and changes on precipitation.

2.2.2 Impacts on Coastal Lagoons

The entrance conditions of coastal lagoons are the main feature that controls the physical processes inside the lagoon. The entrance behavior is driven by the dynamic balance between catchment runoff and ocean wave/beach processes. Climate change is expected to change both rainfall and coastal processes, therefore, wide changes are expected to occur in coastal lagoons (Haines, 2008).

Sea level rise, temperature, precipitation, and storminess are expected to change significantly with global climate change and to impact coastal lagoons (Anthony et al, 2009).

2.2.2.1 Sea level rise

Due to glacial melting and thermal expansion of the oceans, mean sea level, on a global scale, has been increasing over the past century and is expected to keep increasing in the future. IPCC (2007) estimated an increase between 0.18 and 0.79 (including an allowance of 0.2m for the uncertainty related to Ice sheet flow) by the end of 21st century.

Accelerated sea level rise is an important issue especially to low lying shallow-gradient coastal ecosystems. Most barrier-lagoon system responds naturally to sea level rise by migration landward along undeveloped shorelines with gentle slopes. This retreat will lead to steeper and narrower barrier profiles, shortening the length of existing inlets and potentially increasing the rate of exchange with the ocean. Salinity inside the lagoon will probably increase, altering species composition and the ecology of the lagoons. Changes in salt balance of coastal lagoons may change the circulation due to baroclinic processes (Haines, 2008).

Sea level rise may affect cross-sectional inlet stability. For example, a permanently open, inlet may evolve into an intermittently closing inlet; or, a seasonally closing inlet may evolve into a permanently open, inlet. Such changes in inlet condition are highly likely to affect navigability and estuary/lagoon water quality.

Local groundwater tables around the lagoon are expected to rise due to the increase in low tide levels. The typical water depth will also increase, what can cause impacts on benthic ecology, due to less penetration of light, and geochemical processes within the sediments. The increasing of depth may lead to a greater potential for stratification because the decrease of the potential for mixing by wind driven circulation (Haines, 2008).

2.2.2.2 Temperature

Shallow water bodies with slow circulation, such as coastal lagoons, are strongly influenced by changes in air temperature. The increase of air temperature will have more influence in the temperature of coastal lagoons than in open estuaries or the ocean. Water temperature influences dissolve oxygen concentration as well the physiology of lagoon organisms, species ranges and patterns of migration, and can change the ecology of the lagoon (Anthony et al, 2009).

2.2.2.3 Precipitation

There will be changes in precipitation intensity, timing, volume and form due to Global Climate Change. These changes will vary spatially and temporally. Intense precipitation would increase freshwater inputs and locally reduce salinity. Alternatively, lower precipitation would reduce freshwater input and potentially result in higher salinity. Salinity would also be affected by changes in flushing rate, which may counteract the changes in freshwater inputs. Increased freshwater input can also contribute to stratification of deeper lagoons increasing the risk of hypoxia in bottom waters (Anthony et al, 2009).

Other effects of increased surface water inputs include increased delivery of sediment and nutrients to lagoons. Increased nutrient inputs may accelerate eutrophication of lagoons, especially those with low flushing rates. As with sea level rise, increased turbidity will reduce light penetration and the photosynthetic activity of submerged aquatic vegetation, compounding the risk of eutrophication as nutrient dynamics are further altered (Anthony et al, 2009).

2.2.2.4 Storminess

Storms affect lagoons through overwash events and by erosion from wind and waves. There are predictions that the frequency and intensity of extreme weather events have been increasing, and will continue to increase with global temperatures (Anthony et al, 2009).

The consequences of sea level rise become acute during storm events because sea level rise and storms interact to erode barriers and produce high storm surges, rapidly redistributing barrier sediment. During periods of high storm surges, water moves rapidly over the barrier in a process called overwash, which delivers sediment eroded from the front of the barrier onto the back barrier flat and into the lagoon. Increased storm intensity will likely cause more frequent breaches of barrier islands, which in turn will increase the rate of exchange with the ocean, and consequently the flushing rate and salinity of lagoons (Anthony et al, 2009).

3. Study area

3.1. General

Located in the southern part of Thailand around the latitude 7°N and longitude 100°E, Songkhla Lake is the larger natural lagoon in Thailand. It is called a lake, but actually is a shallow water lagoon formed by interaction of land and ocean processes over geological times (Viet et al. 2007). It is considered a choked lagoon according to Kjerfve classification with a mean depth of 1-2m. In some areas, the depth is around 5 to 7m like the channel connecting Thale Luang and Thale Sap Songkhla, called Pak Ro and the channel connecting Thale Sap Songkhla to the ocean, where a navigation channel has been made by dredging. In the vicinity of the lower portion of Thale Sap Songkhla around Ko Yo the depths are between 3 and 4 m (Kjerfve, 1986).

This complex is surrounded by three provinces which are Songkhla, Phatthalung and Nakorn Si Thammarat. The total drainage basin area is 7190 km^2, of which 1043 km^2 is lagoon surface. It is connected with the Gulf of Thailand through a narrow channel at Songkhla town, and it comprises of four sub-lagoons: Thale Noi, Thale Luang, Thale Sap and Thale Sap Songkhla (Figure 4) (Vongvisessomjai, 1999).

There are 8 major canals draining water into the lagoon, namely Khlong Pa Phayom, Khlong Tha Nae, Khlong Na Thom, Khlong Tha Madua, Khlong Pa Bon, Khlong Phru Pho, Khlong Rattaphum and Khlong Utaphao. In addition, there is a swamp in the northern part, Khru Khruan Kreang (Ganasut, 2005).

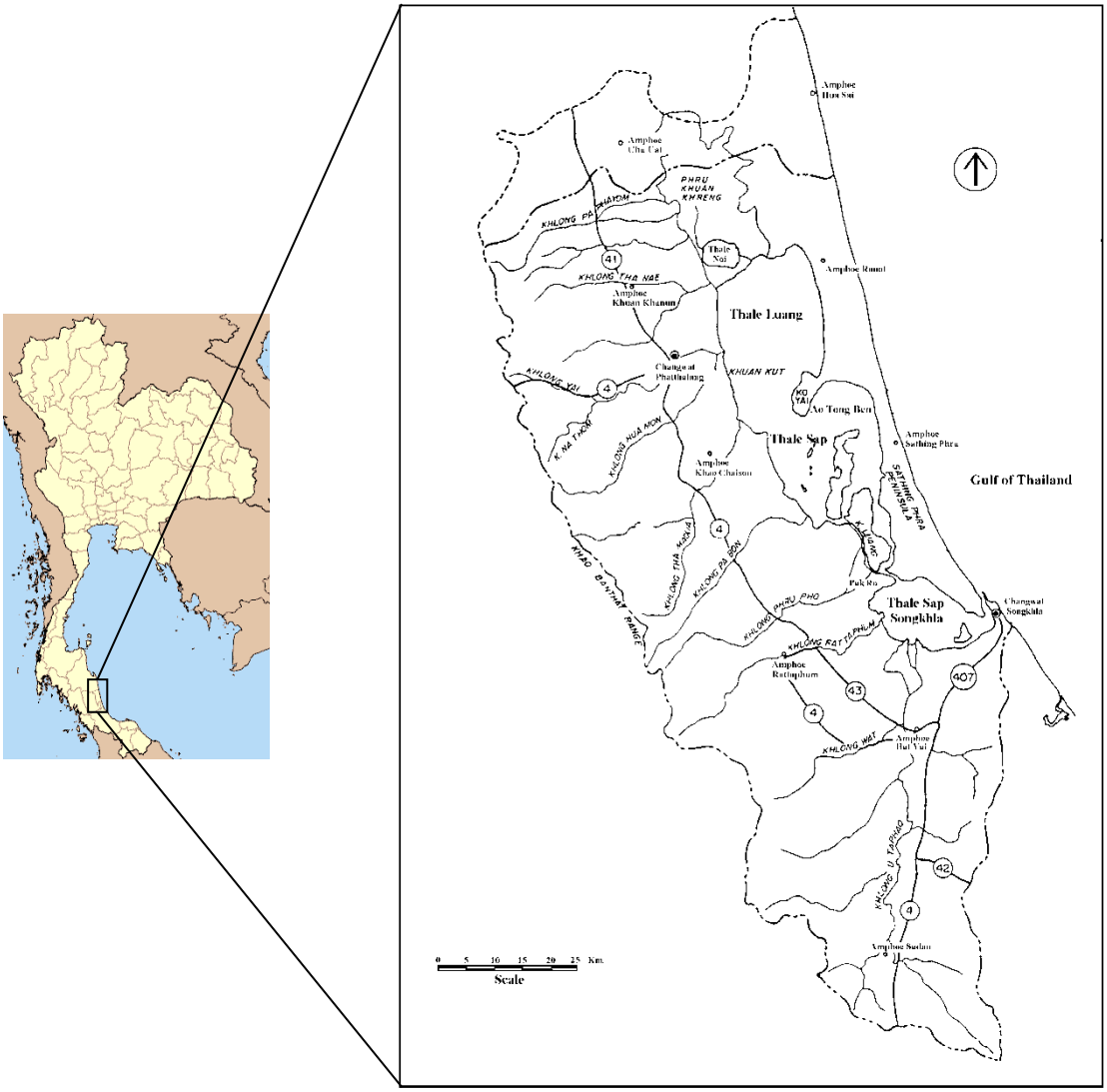

Figure 4 - Map of Songkhla Lagoon

The Songkhla lagoon basin consist of three main topographic units: a narrow range of mountains to the west and south of the basin, foothills and terraces used predominantly for rubber plantations, and broad plains on the east and west sides of the lagoon used mainly for wet season rice production (Vongvisessomjai, 1999).

There is an ample variation in the soil composition of the bed materials, but soft clays are the most frequent. Clay loam is predominant in the northern part of the lagoon while in the southern part silty loan with sandy clay loam is found. In the vicinity of the tidal inlet sand and silt are found on the channel bed especially after dredging of the navigation channel (Vongvisessomjai, 1999).

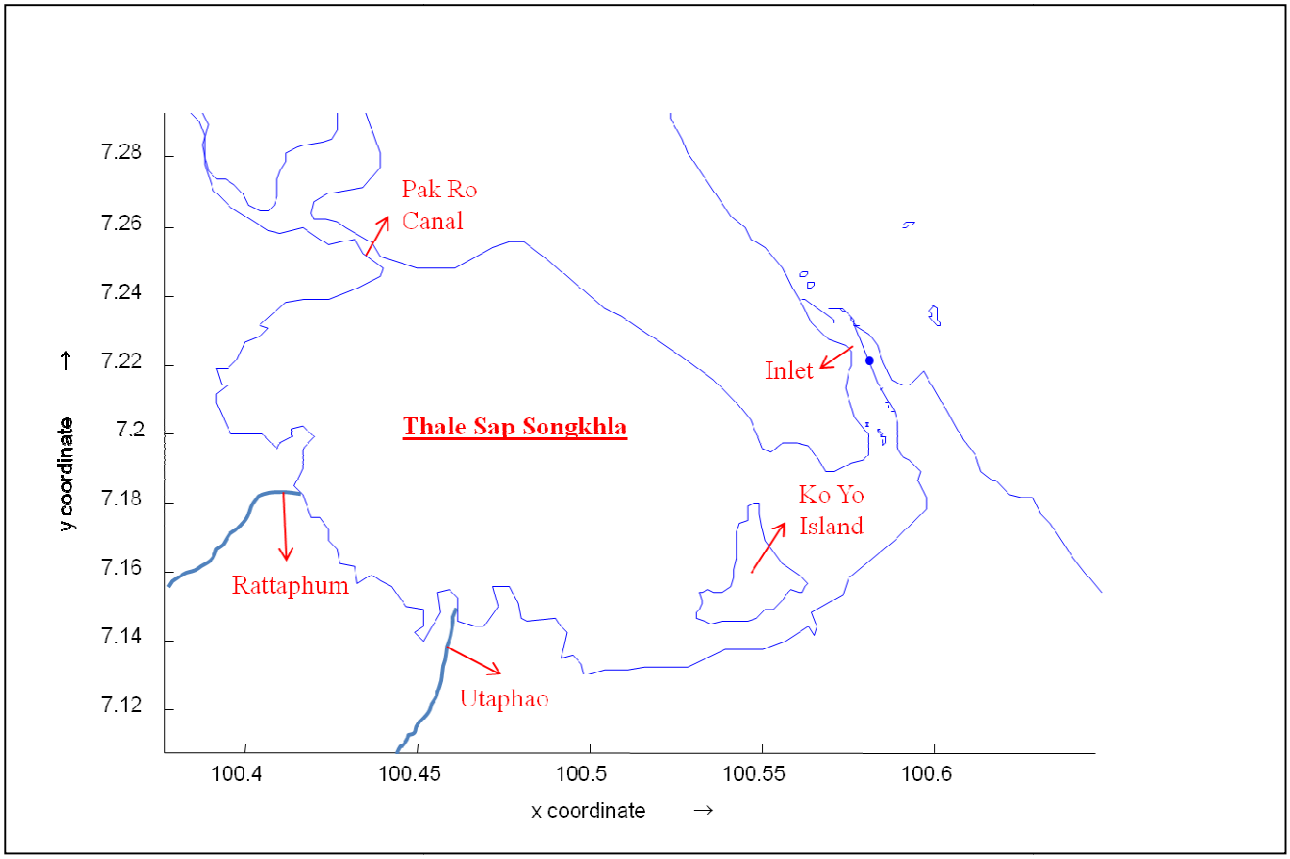

Figure 5 - Thale Sap Songkhla map

This study will focus on Thale Sap Songkhla (Figure 5), which is the southernmost sub-lagoon of Songkhla lagoon and connects the lagoon system with the sea. The total drainage area of the sub-lagoon is 3096km^2, of which 186km^2 is lagoon surface. Two rivers drain directly into the sub-lagoon, Khlong Rattaphum, in the west part and Khlong Utaphao, in the southwest part of the lagoon with a basin area of 2177km^2. Water also enters from the upper sub-lagoons through Pak Ro canal. Close to the entrance of the lagoon, there is an island named Ko Yo. The average depth is 1.3m and the water is brackish to salty varying seasonally (Ganasut, 2004).

3.2. Importance

Songkhla Lake is abundant in aquatic plants and animals. Its rich resources have support fishery and life of people nearby. Aquaculture of sea bass plays an important role in area's economy (Viet, 2007).

3.3. Flow conditions

U-Tapao Canal is the main river discharge of the lagoon and has a catchment area of 2305 km^2. The topography varies from a mild mountainous plateau on the west to the flat fluvial coastal landscape on the

east. The river bed is generally sandy and it has a discharge of 7.8m^3/s in the dry season (March-May) and 88.60m3/s in the wet season (September-November). The width varies from 40 to 80m and the depth from 3 to 8m. The distance from the upper regions to the mouth of the canal is about 70km, with varying channel slopes (Sae-Chew, 2006).

3.4. Climatic conditions

The area is located in a tropical region, which means high temperatures and high humidity during most of the year and two seasons: wet and dry. The climate is governed by two monsoons: the southwest monsoon and the northeast monsoon. According to the statistics of climatological data at Songkhla weather station, in the period of 1971 to 200, the average temperature and relative humidity are respectively, 28.1^{o}C and 76.8%. The average annual rainfall is 1995mm and about 62.1% of the total normally occurs from October to December (Ganasut, 2004).

The wind direction is influenced by the monsoon system. During the months between December and March, the wind direction is predominantly from eastern direction while the period of June to September, it is predominantly from western direction (Figure 6). The other months are transitional seasons. The analysis of data from 1981 to 1997 shows that the lagoon is located in a weak wind zone. Velocities greater of 10 knots occurred only 10% of the time while stronger than 20 knots occurred only 0.01% during the whole 17 year wind record (Ganasut, 2004).

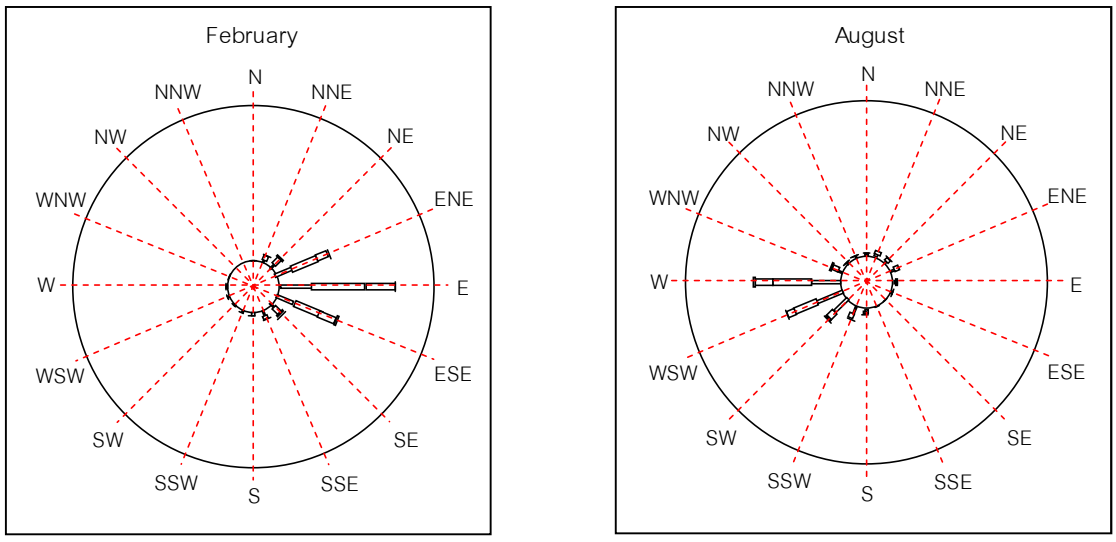

Figure 6 – Prevailing wind direction in the study area (1981-1997)

3.5. Tidal conditions

The tides in the Gulf are mixed and well defined by four tidal constituents, K1, O1, M2 and S2. Harmonic analysis reveals that the tides are strongly dominated by the semi-diurnal constituent (~12.4 h period). The tidal ranges are approximately 30 and 60 cm for neap and spring tides, respectively (Pornpinatepong, 2006).

3.6. Circulation

The complexity of the lake system is governed by tide, runoff, wind and wave. The lake geometry and bathymetry play an important role in the circulation with the currents prevailing in deep channel. The maximum current speed is found in the deep channel of the lake entrance. Pornpinatepong et al. (2006) found a maximum current speed of about 0.75 m/s during june, 1997 at the lake entrance. Due to the island, close to the entrance channel, the flow diverges into two stream paths passing north and south of Ko Yo. Usually, the current of the northern side is stronger than that of the southern side. The tidal wave takes about half an hour to propagate to Pak Ro.

According to Pornpinatepong et al. (2006), there is significant shift in the relative phase between surface elevation and velocity from Ko Yo to Pak Ro. At Ko Yo, the sea surface is 90^{o} out of phase with the currents, and can be considered as a standing wave pattern. At Pak Ro, there is no phase shift between the two measurements, what is a characteristic of a partially progressive wave. This could explain the high complexity of Thale Sap Songkhla hydrodynamic.

Pornpinatepong et al. (2006) also note that there is a gyre near the lake entrance when the flow changes its direction to ebb or flood stage. This gyre persists for less than 30 min and could indicate a sensitive area to human activities.

3.7. Mixing

Usually, complete mixing of seawater and freshwater can be found throughout Southern Lake, except for the deeper sections such as around Pak-ro, Ko Yo, and the lake entrance, where salinity stratification occurs. Normal sea salinity is 32-35 ppt and the seawater flow can cause salinity up to 31 ppt at Ko Yo in the dry season (Pornpinatepong, 2010).

From October to January, in the late rainy season, the freshwater usually flush most of the salt water, and the Southern Lake become almost fresh on the surface, although salinity stratification can persist in the deeper portions. North ok Ko Yo, stratification at 3m deep was found to result in a difference of 12 ppt

between the water surface and the bottom, while as the lake entrance this difference reached 22 ppt. (Pornpinatepong, 2004)

4. Model Description

This chapter is based on Lesser et al, (2004) and the Delft3D-FLOW and WAQ user manuals (2009), and is a summary of the important theory.

Delft3D-FLOW is a multi-dimensional (2D or 3D) hydrodynamic and transport modeling system of Deltares for the aquatic environment which calculates non-steady flow and transport phenomena that result from tidal and meteorological forcing on a rectilinear or a curvilinear, boundary fitted grid. The differential equations solved numerically in the model are: the horizontal momentum equations, the continuity equation, the transport equation, and a turbulence closure model. Vertical accelerations are assumed to be small so the vertical momentum equation is reduced to the hydrostatic pressure relation. In 3D simulations, the vertical grid is defined following the sigma co-ordinate approach.

Delft3D-WAQ is a 3-dimensional water quality model that solves the advection-diffusion-reaction equation and allows great flexibility in the substances to be modeled. It should be coupled to Delft3D-FLOW or another model to get hydrodynamic conditions.

4.1. Hydrodynamic equations

Delft3D-FLOW solves the Navier Stokes equations for an incompressible fluid with shallow water and Boussinesq assumptions. Vertical accelerations are neglected, which leads to hydrostatic pressure equation. Vertical velocities are computed from continuity equation. These differential equations are solved using a finite difference grid with orthogonal curvilinear coordinates.

4.1.1 Continuity equation

The depth average continuity equation is given by:

$$\frac{\partial \zeta}{\partial t} + \frac{1}{\sqrt{G_{\xi\xi}}\sqrt{G_{\eta\eta}}} \frac{\partial \left[(d+\zeta) U \sqrt{G_{\eta\eta}}\right]}{\partial \xi} + \frac{1}{\sqrt{G_{\xi\xi}}\sqrt{G_{\eta\eta}}} \frac{\partial \left[(d+\zeta) U \sqrt{G_{\xi\xi}}\right]}{\partial \eta} = Q$$

Where Q represents the contribution per unit are due to the discharge or withdrawal of water, evaporation, and precipitation and is given by:

$$Q = H \int_{-1}^{0} (q_{in} - q_{out}) d\sigma + P - E$$

Both spherical and orthogonal curvilinear co-ordinates can be used in Delft 3D with the following relations:

$$\sqrt{G_{\xi\xi}} = R\cos\phi$$

$$\sqrt{G_{\eta\eta}} = R$$

$$\xi = \lambda$$

$$\eta = \phi$$

4.1.2 Momentum equations in horizontal direction

The momentum equations in both directions are given by:

$$\frac{\partial u}{\partial t} + \frac{u}{\sqrt{G_{\xi\xi}}}\frac{\partial u}{\partial \xi} + \frac{v}{\sqrt{G_{\eta\eta}}}\frac{\partial u}{\partial \eta} + \frac{\omega}{d+\zeta}\frac{\partial u}{\partial \sigma} - \frac{v^2}{\sqrt{G_{\xi\xi}}\sqrt{G_{\eta\eta}}}\frac{\partial \sqrt{G_{\eta\eta}}}{\partial \xi} + \frac{uv}{\sqrt{G_{\xi\xi}}\sqrt{G_{\eta\eta}}}\frac{\partial \sqrt{G_{\xi\xi}}}{\partial \eta} - fv$$
$$= -\frac{1}{\rho_0\sqrt{G_{\xi\xi}}}P_\xi + F_\xi + \frac{1}{(d+\zeta)^2}\frac{\partial}{\partial \sigma}\left(\nu_V\frac{\partial u}{\partial \sigma}\right) + M_\xi$$

$$\frac{\partial v}{\partial t} + \frac{u}{\sqrt{G_{\xi\xi}}}\frac{\partial v}{\partial \xi} + \frac{v}{\sqrt{G_{\eta\eta}}}\frac{\partial v}{\partial \eta} + \frac{\omega}{d+\zeta}\frac{\partial v}{\partial \sigma} - \frac{u^2}{\sqrt{G_{\xi\xi}}\sqrt{G_{\eta\eta}}}\frac{\partial \sqrt{G_{\xi\xi}}}{\partial \eta} + \frac{uv}{\sqrt{G_{\xi\xi}}\sqrt{G_{\eta\eta}}}\frac{\partial \sqrt{G_{\eta\eta}}}{\partial \xi} + fu$$
$$= -\frac{1}{\rho_0\sqrt{G_{\eta\eta}}}P_\eta + F_\eta + \frac{1}{(d+\zeta)^2}\frac{\partial}{\partial \sigma}\left(\nu_V\frac{\partial v}{\partial \sigma}\right) + M_\eta$$

Where σ is the vertical co-ordinate given by:

$$\sigma = \frac{z-\zeta}{d+\zeta} = \frac{z-\zeta}{H}$$

In the model, the vertical momentum equation is reduced to a hydrostatic pressure equation. For non-uniform density, the following equations are used:

$$\frac{1}{\rho_0\sqrt{G_{\xi\xi}}}P_\xi = \frac{g}{\sqrt{G_{\xi\xi}}}\frac{\partial \zeta}{\partial \xi} + g\frac{d+\zeta}{\rho_0\sqrt{G_{\xi\xi}}}\int_\sigma^0\left(\frac{\partial \rho}{\partial \xi} + \frac{\partial \rho}{\partial \sigma}\frac{\partial \sigma}{\partial \xi}\right)d\sigma'$$

$$\frac{1}{\rho_0\sqrt{G_{\eta\eta}}}P_\eta = \frac{g}{\sqrt{G_{\eta\eta}}}\frac{\partial \zeta}{\partial \eta} + g\frac{d+\zeta}{\rho_0\sqrt{G_{\eta\eta}}}\int_\sigma^0\left(\frac{\partial \rho}{\partial \eta} + \frac{\partial \rho}{\partial \sigma}\frac{\partial \sigma}{\partial \eta}\right)d\sigma'$$

The horizontal Reynold's stresses, F_ξ and F_η are determined using the eddy viscosity concept. For large-scale simulations the forces F_ξ and F_η can be reduced to:

$$F_\xi = \nu_H \left(\frac{1}{\sqrt{G_{\xi\xi}}\sqrt{G_{\xi\xi}}} \frac{\partial^2 u}{\partial \xi^2} + \frac{1}{\sqrt{G_{\eta\eta}}\sqrt{G_{\eta\eta}}} \frac{\partial^2 u}{\partial \eta^2} \right)$$

$$F_\eta = \nu_H \left(\frac{1}{\sqrt{G_{\xi\xi}}\sqrt{G_{\xi\xi}}} \frac{\partial^2 v}{\partial \xi^2} + \frac{1}{\sqrt{G_{\eta\eta}}\sqrt{G_{\eta\eta}}} \frac{\partial^2 v}{\partial \eta^2} \right)$$

M_ξ and M_η represent the contributions due to external sources or sinks of momentum and are given by:

$$M_\xi = q_{in(\hat{U}-u)}$$

$$M_\eta = q_{in(\hat{V}-v)}$$

4.1.3 Vertical velocities

The vertical velocity is computed from the continuity equation. These velocities can be expressed in the horizontal velocities, water depths, water levels and ω-vertical according to:

$$w = \omega + \frac{1}{\sqrt{G_{\xi\xi}}\sqrt{G_{\eta\eta}}} \left[u\sqrt{G_{\eta\eta}} \left(\sigma \frac{\partial H}{\partial \xi} + \frac{\partial \zeta}{\partial \xi} \right) + v\sqrt{G_{\xi\xi}} \left(\sigma \frac{\partial H}{\partial \eta} + \frac{\partial \zeta}{\partial \eta} \right) \right] + \left(\sigma \frac{\partial H}{\partial t} + \frac{\partial \zeta}{\partial t} \right)$$

4.1.4 Transport equation

$$\frac{\partial (d+\zeta)c}{\partial t} + \frac{1}{\sqrt{G_{\xi\xi}}\sqrt{G_{\eta\eta}}} \left\{ \frac{\partial \left[\sqrt{G_{\eta\eta}} (d+\zeta) uc \right]}{\partial \xi} + \frac{\partial \left[\sqrt{G_{\xi\xi}} (d+\zeta) vc \right]}{\partial \eta} \right\} + \frac{\partial \omega c}{\partial \sigma}$$

$$= \frac{d+\zeta}{\sqrt{G_{\xi\xi}}\sqrt{G_{\eta\eta}}} \left\{ \frac{\partial}{\partial \xi} \left[\frac{D_H}{\sigma_{c0}} \frac{\sqrt{G_{\eta\eta}}}{\sqrt{G_{\xi\xi}}} \frac{\partial c}{\partial \xi} \right] + \frac{\partial}{\partial \eta} \left[\frac{D_H}{\sigma_{c0}} \frac{\sqrt{G_{\xi\xi}}}{\sqrt{G_{\eta\eta}}} \frac{\partial c}{\partial \eta} \right] \right\}$$

$$+ \frac{1}{d+\zeta} \frac{\partial}{\partial \sigma} \left[\frac{\nu_{mol}}{\sigma_{mol}} + max \left(\frac{\nu_{3D}}{\sigma_c}, D_V^{back} \right) \frac{\partial c}{\partial \sigma} \right] - \lambda_d (d+\zeta) c + S$$

Where S represents the source and sink terms per unit area due to the discharge or withdrawal of water, and the exchange of heat through the free surface, given by:

$$S = (d+\zeta)(q_{in} c_{in} - q_{out} c) + Q_{tot}$$

The horizontal and vertical viscosity (ν_H and ν_V) and diffusivity (D_H and D_V) need to be prescribed. The model assumes that the horizontal viscosity is a superposition of three parts: a part due to "sub-grid scale turbulence", a part due to "3D-tubulence" and a part due to dispersion.

$$\nu_H = \nu_{SGS} + \nu_{3D} + \nu_H^{back}$$

And

$$\nu_V = \nu_{mol} + max\left(\nu_V^{back}, \nu_{3D}\right)$$

Table 1 summarizes how Delft3D-FLOW calculates these terms

Table 1 – Delft 3D calculations of viscosity terms

Model description	ν_{SGS}	ν_H^{back}	ν_{3D}	ν_V^{back}
2D, no HLES	-	2D-turbulence + dispersion coefficient	-	-
2D, with HLES	Computed by HLES	3D-turbulence + dispersion coefficient	-	-
3D, no HLES		2D-turbulence	Computed by vertical turbulence model	Background vertical viscosity
3D, with HLES	Computed by HLES	-	Computed by vertical turbulence model	Background vertical viscosity

Typically, the horizontal eddy diffusivity D_H exceeds the vertical eddy diffusivityD_V. The horizontal diffusion coefficient is assumed to be a superposition of three parts: the 2D part due to motions and mixing not resolved by the horizontal grid ("subgrid scale-turbulence"), the contribution due to 3D turbulence and the D_H^{back} by solving the Reynolds-averaged equations and/or accounting for other unresolved horizontal mixing.

$$D_H = D_{SGS} + D_{3D} + D_H^{back}$$

And the vertical eddy diffusivity coefficient is defined by:

$$D_V = \frac{\nu_{mol}}{\sigma_{mol}} + max\left(D_V^{back}, D_{3D}\right)$$

The 3D-turbulence part is defined as the minimum of the vertical eddy diffusivity computed by the turbulence model and the Ozmidov length scale:

$$D_{3D} = max\left(D_{3D}, 0.2L_{oz}^2\sqrt{-\frac{g}{\rho}\frac{\partial\rho}{\partial z}}\right)$$

Summarizing, in the model many options are available for the eddy diffusivity, table presents an overview of these options:

Table 2 - Delft 3D calculations for diffusivity terms

Model description	D_{2D}	D_H^{back}	D_{3D}	D_V^{back}
2D, no HLES	0	2D-turbulence + dispersion coefficient	-	-
2D, with HLES	Computed by HLES	3D-turbulence + dispersion coefficient	-	-
3D, no HLES	0	2D-turbulence	Maximum turbulence model and Ozmidov length scale*2	Background eddy diffusivity
3D, with HLES	Computed by HLES	-	Maximum turbulence model and Ozmidov length scale*2	Background eddy diffusivity

4.1.5 Turbulence closure models

Four turbulence closure models have been implemented in Delft3D-FLOW to determine ν_V and D_V: Constant coefficient, Algebraic Eddy viscosity closure Model (AEM), k-L turbulence closure model and k-ε turbulence closure model. They are all based on the "eddy viscosity" concept. The eddy viscosity in the models has the following form:

$$\nu_V = c'_\mu L\sqrt{k}$$

Where c'_μ a constant determined by calibration, L is is the mixing length, and k is the turbulent kinetic energy.

In the present work, the model was set with the k-ε turbulence closure model, which is a second order turbulence model. In this model both the turbulent energy k and the dissipation ε are produced by production terms representing shear stresses at the bed, surface, and in the flow. The transport equation is used then to calculate the "concentration" of these terms. The mixing length is determined by:

$$L = c_D \frac{k\sqrt{k}}{\varepsilon}$$

4.2. Boundary conditions

In order to solve the system with differential equations and get a unique solution, a set of initial and boundaries conditions for water levels and horizontal velocities are required. Natural boundaries like river banks and coast lines are called closed boundaries and the flow velocities normal to these boundaries are equal to zero. Artificial boundaries "water-water" are called open boundaries and they should be located as far as possible from the area of interest.

4.2.1 Bed and free surface boundary conditions

In the σ-coordinate system, the bed and the free surface correspond with σ-planes. ω is the vertical velocity relative to the σ-plane. Considering the impermeability of the surface and the bottom, the following kinematic conditions are prescribed:

$$\omega|_{\sigma=-1} = 0$$

$$\omega|_{\sigma=0} = 0$$

At the seabed, the boundaries conditions for the momentum equations are:

$$\frac{\nu_V}{H}\frac{\partial u}{\partial \sigma}\bigg|_{\sigma=-1} = \frac{1}{\rho_0}\tau_{b\xi}$$

$$\frac{\nu_V}{H}\frac{\partial v}{\partial \sigma}\bigg|_{\sigma=-1} = \frac{1}{\rho_0}\tau_{b\eta}$$

Where $\tau_{b\xi}$ and $\tau_{b\xi}$ are bed shear stress components.

4.2.2 Lateral boundary conditions

Along closed boundaries, the velocity component perpendicular to the closed boundary is set to zero. For the shear stress along the boundary one of the following conditions can be prescribed: zero tangential shear-stress or partial slip

At open boundaries, one of the following types of boundary conditions must be specified: water level, velocity, discharge, Neumann, or Riemann invariant. For the velocity and discharge type of boundary condition, the flow is assumed to be perpendicular to the open boundary. In 3D models you can prescribe: a uniform profile, a logarithmic profile or a 3D profile.

4.2.3 Transport boundary conditions

The horizontal transport of dissolved substances is dominated by advection. Without diffusion, the equation has only one characteristic, which is parallel to the flow. During inflow, a open boundary is needed, while during outflow, the concentration must be free. The vertical profile can be of four types: uniform profile, linear profile, step profile or 3D profile.

4.3. Numerical solution

Delft3D-FLOW is a numerical model based on finite differences. The equations are discretized in space, by covering the area with a curvilinear grid, which is assumed to be orthogonal and well-structured. The grid co-ordinates can be Cartesian or spherical. The variables are arranged in a pattern called the Arakawa C-grid (a staggered grid). In this pattern, the water level points are defined in the center of a cell, and the velocities components are perpendicular to the grid cell faces where they are situated.

In the vertical direction, two types of grid are available: a boundary fitted σ co-ordinates or a grid that is strictly horizontal called the Z-grid

4.3.1 Hydrodynamics

The numerical method used to solve the continuity and the horizontal momentum equations is an alternating direction implicit method (ADI). The main advantage of this method is that the implicitly integrated water levels and velocities are coupled along grid lines, leading to systems of equations with a small band width. In order to have stability, the scheme denoted “cyclic method” was implemented. This method splits one time step into two stages. The time levels in these stages are alternating, if in one stage a term is taken implicitly in time, this term will be taken explicitly in time in the next stage. For the complete time step, each separate term is still integrated second-order accurate in time. First the water

levels are computed and then they are substituted in the discrete momentum equations, given the velocities. This leads to a method that is computationally efficient, at least second-order accurate, and stable at Courant numbers of up to approximately 10.

In vector form the ADI-method is given by:

Step 1:

$$\frac{\vec{U}^{l+\frac{1}{2}} - \vec{U}^{l}}{\frac{1}{2}\Delta t} + \frac{1}{2}A_x\vec{U}^{l+\frac{1}{2}} + \frac{1}{2}A_y\vec{U}^{l} + B\vec{U}^{l+\frac{1}{2}} = \vec{d}$$

Step 2:

$$\frac{\vec{U}^{l+1} - \vec{U}^{l+\frac{1}{2}}}{\frac{1}{2}\Delta t} + \frac{1}{2}A_x\vec{U}^{l+\frac{1}{2}} + \frac{1}{2}A_y\vec{U}^{l+1} + B\vec{U}^{l+1} = \vec{d}$$

$$A_x = \begin{bmatrix} 0 & -f & g\frac{\partial}{\partial x} \\ 0 & u\frac{\partial}{\partial x} + v\frac{\partial}{\partial y} & 0 \\ H\frac{\partial}{\partial x} & 0 & u\frac{\partial}{\partial x} \end{bmatrix}$$

$$A_y = \begin{bmatrix} u\frac{\partial}{\partial x} + v\frac{\partial}{\partial y} & 0 & 0 \\ f & 0 & g\frac{\partial}{\partial y} \\ 0 & H\frac{\partial}{\partial y} & v\frac{\partial}{\partial y} \end{bmatrix}$$

$$B = \begin{bmatrix} \lambda & 0 & 0 \\ 0 & \lambda & 0 \\ 0 & 0 & \lambda \end{bmatrix}$$

Where λ is the linearized bottom friction coefficient and $\vec{d}$ is a vector containing external forcing like wind and atmospheric pressure.

4.3.2 Transport

The transport equation is formulated in a conservative form (finite-volume approximation) and is solved using the "cyclic method". For steep bottom slopes in combination with vertical stratification, horizontal diffusion along σ-planes introduces artificial vertical diffusion. DELFT3D-FLOW includes an algorithm to approximate the horizontal diffusion along z-planes in a σ-coordinate framework. In addition, a horizontal Forester filter, based on diffusion along r-planes is applied to remove any negative concentration values that may occur. The Forester filter is mass conserving and does not cause significant amplitude losses in sharply peaked solutions.

5. Data Analysis

The available data is summarized in Table 3 and the locations are showed in Figure 7 and Figure 8. Bathymetry and Land Boundary data were also available.

Table 3 - Data available information

Data	Point	Latitude	Longitude	Depth	Period
Water level	Songkhla	7.21ºN	100.58ºE	8m	1986-2006
Water level	Pattani	6.9ºN	101.27ºE	1m	1987-2008
Velocity	North of Ko Yo	7.186°N	100.55ºE	4m	29th June – 1st July (1997)
Velocity	South of Ko Yo	7.14°E	100.55ºE	2m	27th – 29th June (1997)
Salinity	Point A	7.174°N	100.544ºE	1m	8th – 11th October (2006)

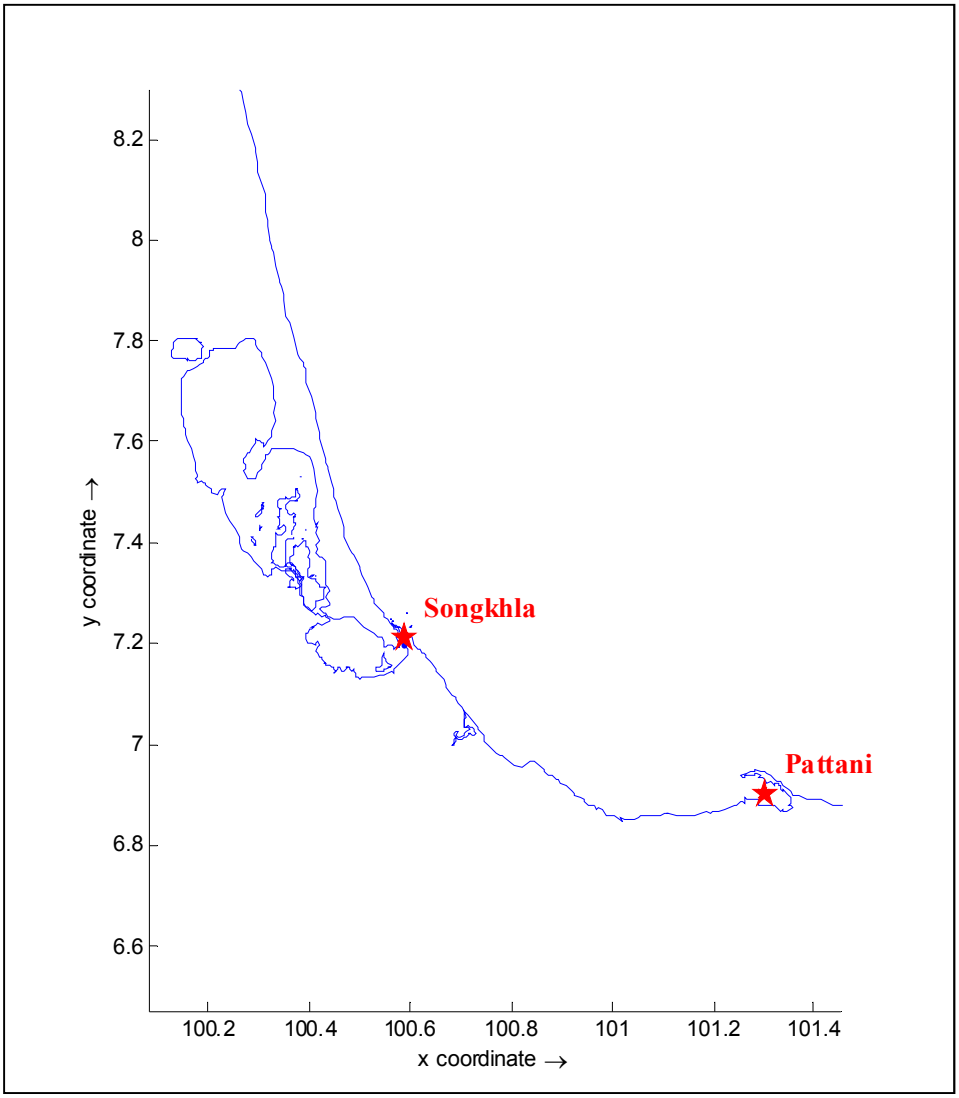

Figure 7 - Locations of Water Level Data

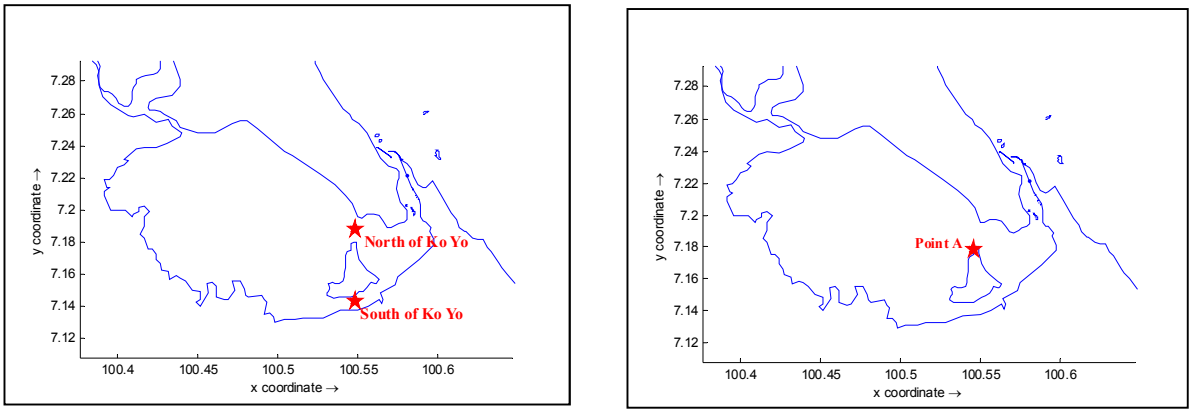

Figure 8 - Location of Velocity (left) and Salinity (risgh) Data of Songkhla Lagoon

5.1. Water Level

Around 21 years of hourly water level data is available for two points: Songkhla and Pattani. The Songkhla point is located in the inlet, while the Pattani point is located in a bay (Figure 7). Both of them do not represent the ocean fluctuations without disturbance, as they are located in shallow, protected areas. Nevertheless, Pattani point is located in an area more exposed than Songkhla point.

A spectral analysis was performed in order to analyze the data (Figure 9). The results show that both locations have similar spectral components for water level data. There are three important cycles: an annual, a semidiurnal and a diurnal. The annual cycle is probably related to the monsoon climate, while the semidiurnal and diurnal cycles are related to tides. According to the figure, the energy related to the annual cycle is almost the same for both points, while the data from Pattani shows more energy on the high frequencies compared to Songkhla. The different exposure to ocean fluctuations can explain this difference; the high frequencies are filtered by the inlet before reaching the Songkhla measurement point.

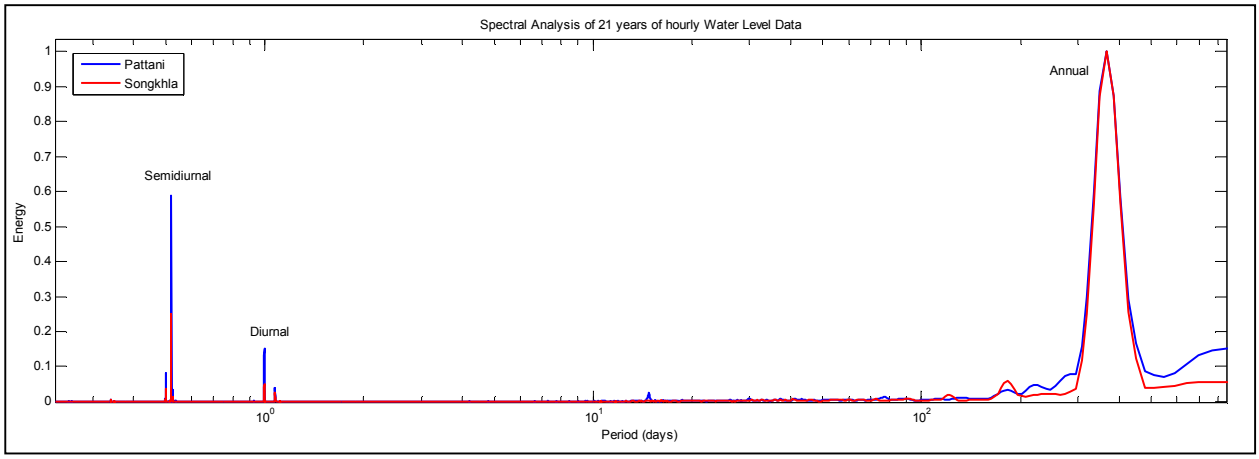

Figure 9 - Spectral Analysis of 21 years of hourly Water Level Data for Pattani and Songkhla. The principal components are also indicated: semidiurnal, diurnal and annual.

To analyze the annual cycle, the two series of data were filtered with a low pass filter which removed all signals with periods less than 4 days. Figure 10 shows the 21 years of this filtered data and also the mean with the standard deviation. The figures show that the annual cycle has amplitude of around 0.5m for both locations. The water level reaches its minimum during the dry season, from June to August and maximum during the wet season, from November to December. The wet season is also the period with higher variability over the years.

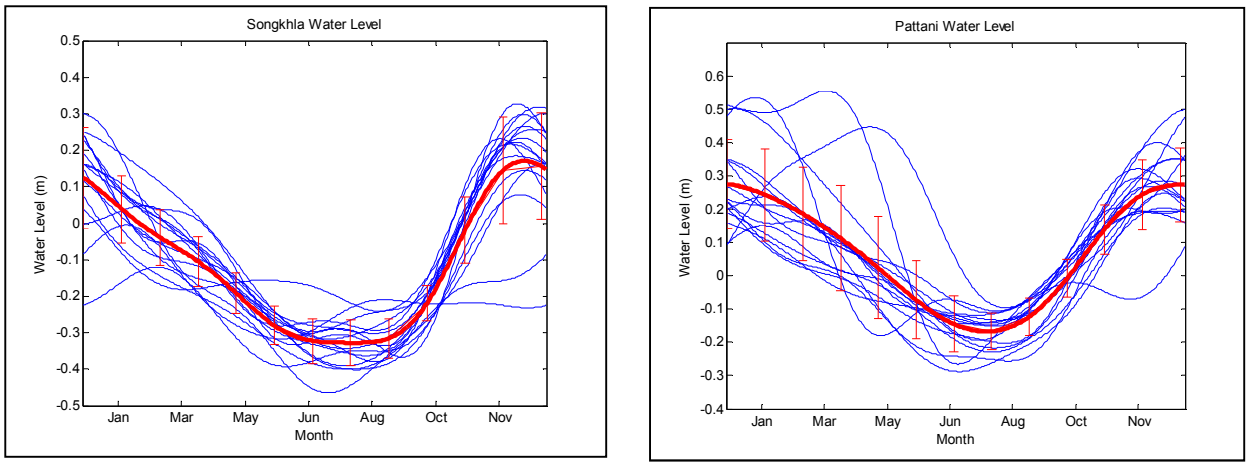

Figure 10 - Monthly Mean Water Level at Songkhla Lagoon (left) and Pattani (right). Blue lines: 21 years of filtered water level data. Red lines: Monthly Mean water level for 21 years of data for both locations and its respective standard deviation.

The water level for the period of October was analyzed and compared for both locations (Figure 11). Both curves are very similar, and have a correlation coefficient of 0.93. The maximum tidal range is about 0.7m for Pattani and 0.6 for Songkhla during spring tides.

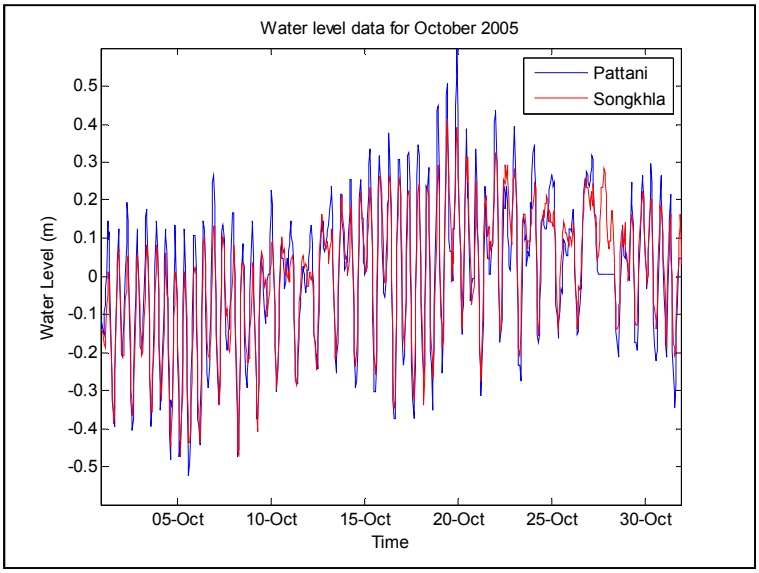

Figure 11 - Water Level Data of the two stations for the period October 2005. The mean is subtracted from the data prior to plotting for comparison.

In order to determine the harmonic components of the tides for the two points, three different methods were used and compared: World tides routine, T tide routine and Delft Dashboard. The four main tidal components (O1, K1, M2 and S2) were analyzed and each amplitude and phase compared to check which method reproduces the data better.

World Tides is a general purpose program for the analysis and prediction of tides. Using least squares harmonic analysis, it allows the user to decompose a water level record into its tidal and non-tidal components by fitting between 5 and 35 user-selectable tidal frequencies (tidal harmonic constituents).

The T TIDE program is a Matlab package used for tidal analysis. The package is the Matlab version of widely-used program for performing harmonic analysis of oceanic tides using FORTRAN created by Mike Foreman (Pawlowicz, 2002).

Delft Dashboard is a standalone Matlab based graphical user interface aimed at supporting modelers in setting up new and existing models. It includes some tidal data, and a tool to estimate tides for any point in the world.

The results are summarized in Figure 12 and show that T tide and World Tides are correlated but Delft Dashboard gives a different result. Unlike the other methods, Delft Dashboard uses built-in assimilation data and doesn't include the obtained data in its analysis, which is probably the reason for this difference. Taking the components from T tide and World tide and comparing them to the original data, the method with better approximation is the World Tides and thus this will be the one used in further analysis.

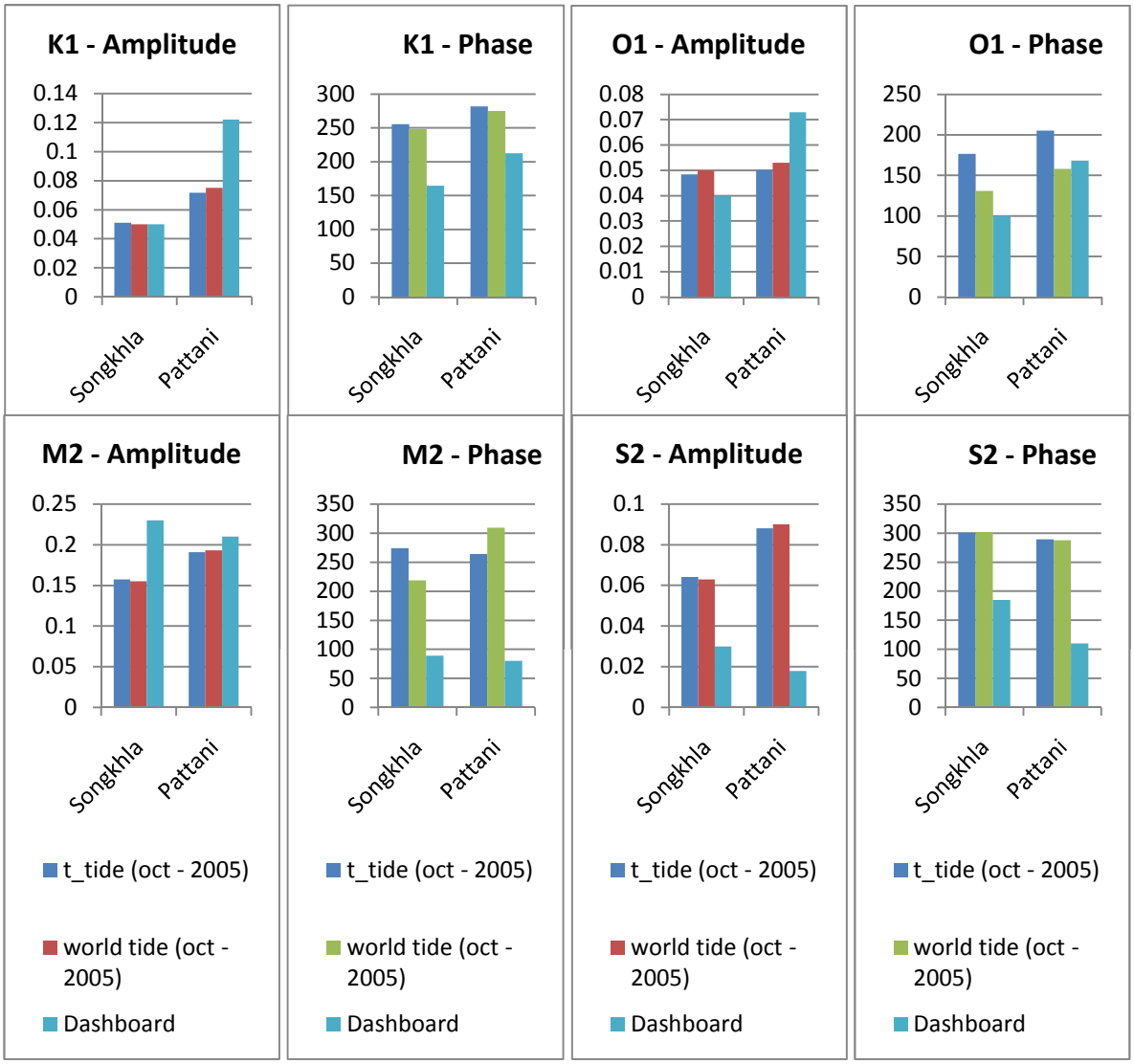

Figure 12 - Principal Harmonic Components (Amplitude and Phase) for the two locations using three different methods (T tide, World tides and Delft Dashboard)

The components given by World Tides show that the main component of the two locations is M2, followed by S2 (Table 4). The amplitudes of the components at Pattani are higher than at Songkhla, and this difference occurs specially with the semidiurnal components. There is a difference in phase for all the components.

Table 4 - Principal Harmonic Components of Songkhla and Pattani

	Amplitude (m)		Phase (°)	
Component	Songkhla	Pattani	Songkhla	Pattani
K1	0.05	0.075	248	274
O1	0.05	0.053	131	158
M2	0.155	0.193	219	309
S2	0.063	0.09	302	288

5.2. Velocity

Velocity data was digitalized from Pornopinatepong et. al. (2006). Current measurements of two points were conducted during the dry season during 6 days of 1997. The two points are located in the two channels formed by the island, one at the north and the other one at the south of the Ko Yo island.

The observed tidal current fluctuation north of Ko Yo Island in June 1997, shows a maximum current speed of about 40cm/s during flood tide (Figure 13). South of Ko Yo the maximum registered was about 30cm/s.

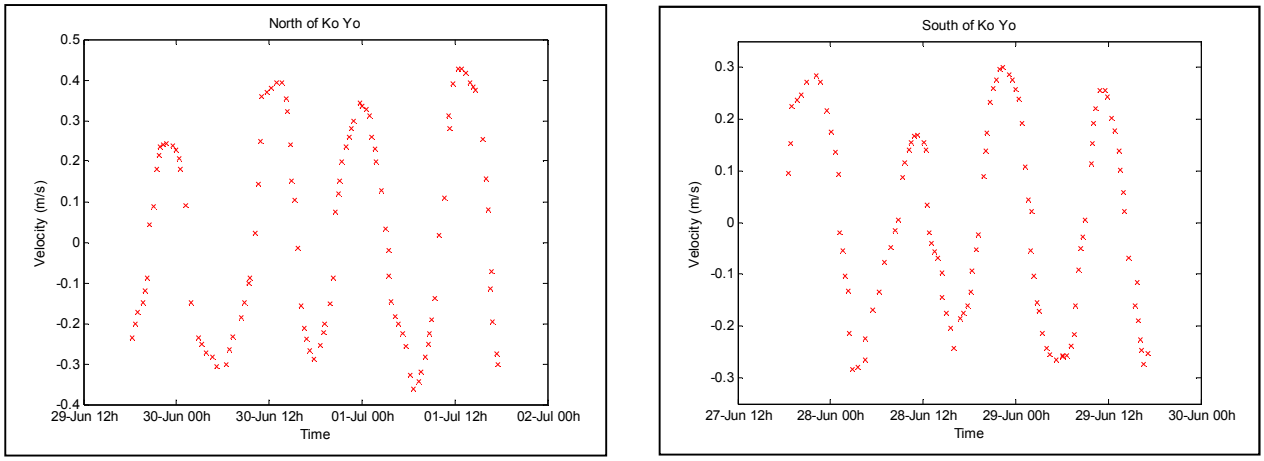

Figure 13 - Velocity Data for two locations. North of Ko Yo Island (left) and South of Ko Yo Island (right)

5.3. Salinity

Salinity data was digitalized from Viet et. al. (2007). Salinity measurements of one point were conducted during October of 2006, during 3 days. The point is located very close to the island in a very shallow area.

The observed salinity fluctuation at point A, shows a maximum salinity of about 32.4 psu and a minimum of about 31(Figure 14).

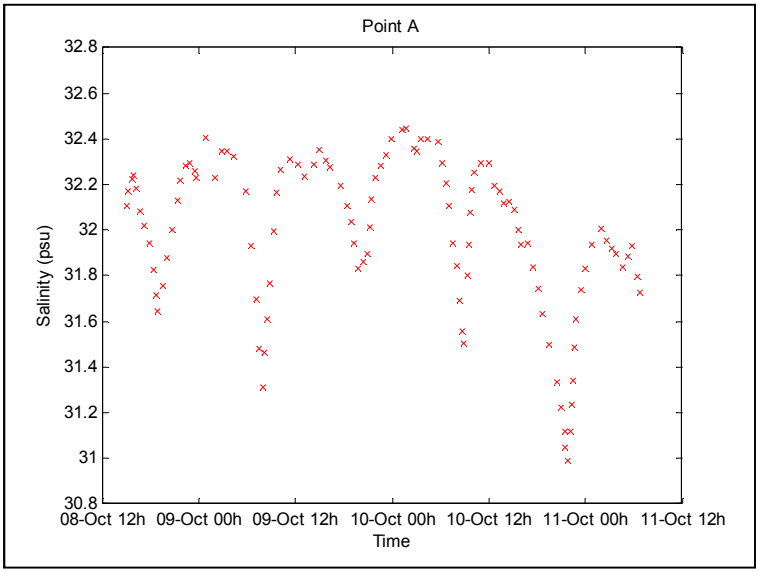

Figure 14 – Salinity Data for Point A

5.4. Modeled Stream flows

The results of two global models ECHAM and GFDL were downscaled to the region of interest.

ECHAM is a Global Climate Model developed by the Max Planck Institute for Meteorology, one of the research organizations of the Max Planck Society. It has its original roots in global forecast models developed at ECMWF. This model has been modified for climate research and is a comprehensive general circulation model of the atmosphere. The model resolves the atmosphere up to 10 hPa and has been used extensively to study the climate of the troposphere.

GFDL CM2.X (Geophysical Fluid Dynamics Laboratory Coupled Model, version 2.X) is a coupled atmosphere-ocean general circulation model developed at the NOAA Geophysical Fluid Dynamics Laboratory in the United States. It is one of the leading climate models used in the Fourth Assessment Report of the IPCC.

The two models show very different results for the stream flow of Songkhla Lagoon for 2000 and 2100 simulations (Figure 15). Considering the year of 2000, the two models have the same behavior, but are different in absolute values. Both of them have a maximum from September to November and a minimum from January to March. They also show a local minimum from July to August. However, the maximum of ECHAM model is around 130m^3/s while GFDL have a maximum around 100m^3/s. The standard deviations of both models are very high.

Considering the year of 2100, the models show different results. Compared to present conditions, ECHAM forecast show an increase of streamflow for most of the year, while GFDL show a decrease of streamflow in most of months.

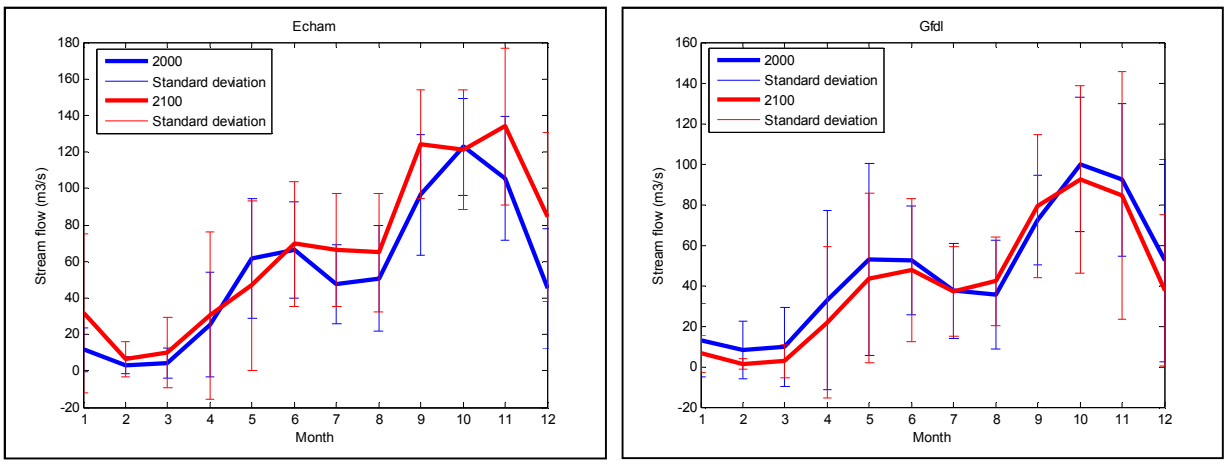

Figure 15 - Monthly Averages Stream flow for Songkhla Lagoon and its respective standard deviation using two different Global Models: ECHAM (left) and GFDL (rigth). The curves were obtained by averaging 20 years of simulations for each period. The blue curve in both figures represents the average of the period 1981-2000 and the red represents the period 2081-2100.

The difference between the results of these two models is an indicator of how variable the models are for river streamflows. These models are based on a lot of assumptions, and probably most of them are not totally correct. Besides all the assumptions of the models, these values are based on models of precipitation/evaporation and don't take into account factors such as irrigation use, or human consumption. In this case study, this might cause large errors.

The values represent the stream flow for the whole basin. For this lagoon, this flow is drained into two main rivers: Rattaphum and Khlong Utaphao. From literature (Ganasut, 2004) it is known that Khlong Utaphao has a flow 4 times greater than Rattaphum. To represent the wet season, the maximum stream flow was taken, and the dry season, the minimum was taken. Using this information, the stream flow was divided as Table 5.

Table 5 - River Flow for the two rivers using GFDL and ECHAM for four periods: 2000 (wet and dry) and 2100 (wet and dry)

	GFDL				ECHAM			
Year	2000		2100		2000		2100	
Season	wet	dry	wet	dry	wet	dry	wet	dry
Total Flow	100	8	92	1.3	122	3	134	6.5
Utaphao	80	6.4	73.6	1.04	97.6	2.4	107.2	5.2
Rattaphum	20	1.6	18.4	0.26	24.4	0.6	26.8	1.3

6. Application for Songkhla Lagoon

6.1. Grid

The optimal grid size is a balance between the computation effort and the physical processes of interest. The model grid should be fine enough to reproduce the processes present in the space scale of interest. However, the computation effort increases with decreasing grid size.

The curvilinear model grid was constructed in a spherical coordinate system with the total of 10159 grid cells using the Delft3D-RGFGRID. The grid size varies in space such that finer grids are located in the inlet and coarser grids are located in the northern part of the lake (Figure 16).

The grid is in agreement with the conditions specified by the Delft3D-RGFGRID User Manual for Orthogonality, M-Smoothness, N-Smoothness and Aspect Ratio.

Table 6 - Characteristics of the grid

Grid size	$\sqrt{G_{\xi\xi}}$	$\sqrt{G_{\eta\eta}}$
Maximum	370m	420m
Minimum	20m	30m

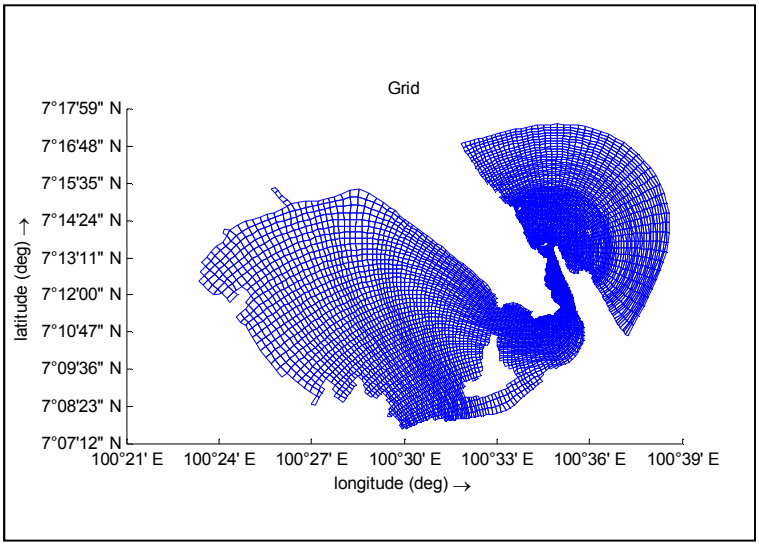

Figure 16 – Grid Configuration

6.2. Bathymetry

The bathymetry inside the lagoon has a average depth of 1.5m. Most of the lagoon has a depth around 2m, in the entrance channel the depth is around 8m. This channel divides into two near the island; the north part has a depth greater than the south part. Pak Ro, the channel which connects Thale Luang with Thale Sap Songkhla is also relatively deep. Outside the lagoon, 7km from the entrance channel, the depth reaches 13m. To setup the bathymetry file, the data was interpolated using Delft3D-QUICKIN (Figure 17).

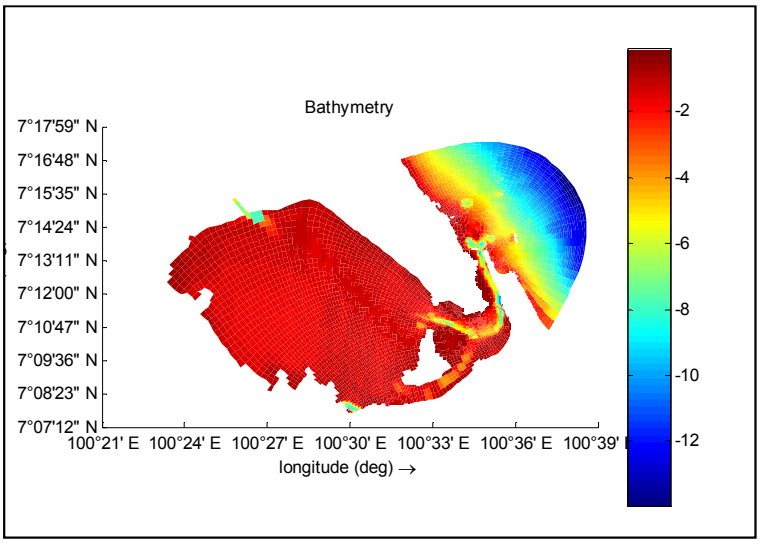

Figure 17 - Bathymetry of Songkhla Lagoon

6.3. Boundary conditions

In this study, two types of open boundaries were used: Water level and Total discharge. Water level was used in the ocean boundary (northeast of the domain). Astronomic components with its respective corrections were used to force this boundary. River discharge was used in the other two open boundaries where the rivers of the domain are present, time series of river discharge were used in these cases. The boundary in the south part of the lagoon represents the river Khlong Utaphao, while the one in the western part represents the river Khlong Rattaphum (Figure 18).

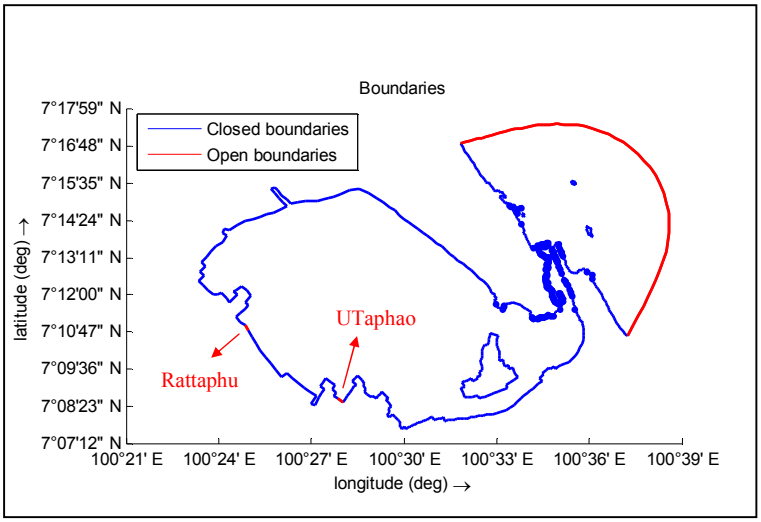

Figure 18 - Boundaries of the domain

6.4. Calibration

6.4.1 Time step

To determine the optimum time step (i.e the largest time step that produces consistent results), five model simulations with different time steps were done: 12 seconds, 30 seconds, 1 minute, 2 minutes and 5 minutes. The spectrum of the results of salinity, water level and velocity for two points, one inside the lagoon and the other one in the inlet, were then compared. The Correlation Coefficient between all the results was calculated and a criteria of Correlation Coefficient greater than 0.95 was adopted to characterize a good correlation.

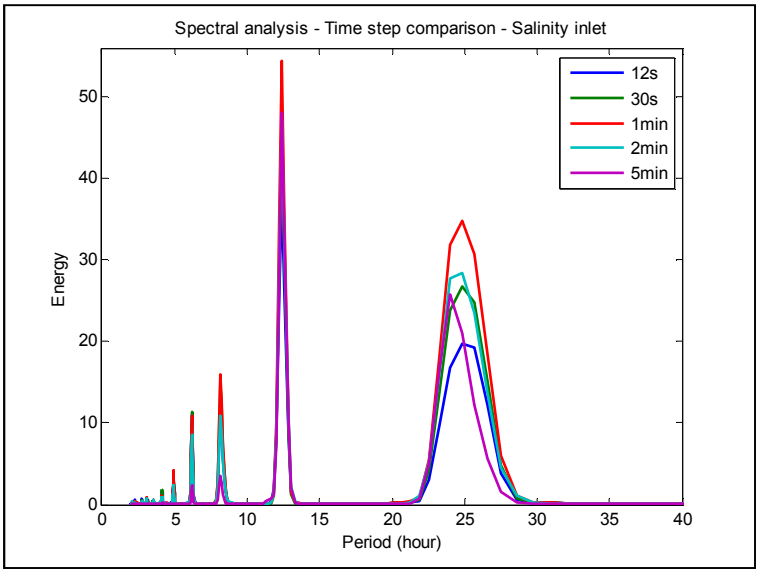

Figure 19 - Spectral Analysis of the results of salinity at the inlet for different time steps simulations

Table 7 - Correlation Coefficient between the results of salinity at the inlet for different time step simulations

Time step	12s	30s	1min	2min	5min
12s	1.0000	0.9792	0.9360	0.8906	0.7926
30s		1.0000	0.9714	0.9225	0.8183
1min			1.0000	0.9608	0.8348
2min				1.0000	0.8565
5min					1.0000

Considering the criteria of correlation adopted, the results show that for velocity and water levels, the model is consistent even for the greatest time step (5 minutes). For salinity, time steps of 2 and 5 minutes were not well correlated with the results of the other time steps. The conclusion is a time step of 30 seconds is the optimum time step for this case.

6.4.2 Eddy viscosity/diffusivity

Eddy viscosity is the turbulent transfer of momentum by eddies, while eddy diffusivity is the exchange coefficient for the diffusion of a conservative property by eddies in a turbulent flow. These two constants are parameters that need to be set in Delft3D-FLOW. To determine both parameters three test cases were simulated:

- Eddy viscosity=0.1 m^2/s and Eddy diffusivity=0.05 m^2/s
- Eddy viscosity=1 m^2/s and Eddy diffusivity=0.5 m^2/s
- Eddy viscosity=10 m^2/s and Eddy diffusivity=5 m^2/s

Water level and velocities almost don't change with the different configurations. However, results for the center of lagoon (Figure 20) show that eddy viscosity and eddy diffusivity have high influence on salinity. Decreasing both parameters, the salinity increases in absolute values and also in amplitude. The salinity data available show that the salinity amplitude is better represented by the combination of Eddy viscosity=0.1 m^2/s and Eddy diffusivity=0.05 m^2/s.

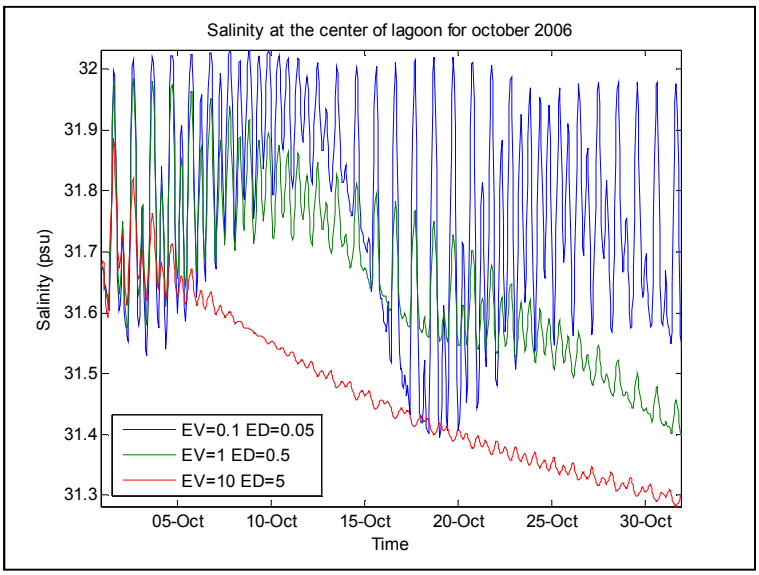

Figure 20 – Salinity comparison at the center of the lagoon for three different combination of Eddy Viscosity and Eddy Diffusivity for October 2006.

6.4.3 Water Level

To calibrate the model for water level, the available water level data for two points were used: Pattani and Songkhla. Pattani data was used determine the boundary condition, while Songkhla data was used to calibrate the model. Firstly, World Tides was used to determine Pattani harmonic constants for June 1997. For each component, there was a difference between the World Tides phase and Delft3D phase. This phase shift was determined by analyzing the results of a point in the boundary with the World Tides and compare with the phase set as input. The corrections for each component are shown in Table 8. The exact reason for this phase shift is still unknown, but probably is related to a different reference date.

Table 8 – Harmonic Components with respectives corrections of Pattani for June 1997.

Constants	Amp (W)	Factor	Phase (W)	Correction	Model amp.	Model Pha.
O1	0.041	1.1	174.3	+46	0.045	220.3
K1	0.118	1.1	291.3	+8	0.130	299.3
N2	0.034	1.5	113.9	-222	0.051	251.3
M2	0.177	1.5	221.2	+55	0.265	276.2
S2	0.037	1.5	314.3	-	0.055	314.3

In order to compare data with model results, Songkhla data was filtered with a high pass filter to eliminate long period signals that are not related with tides (Figure 21).

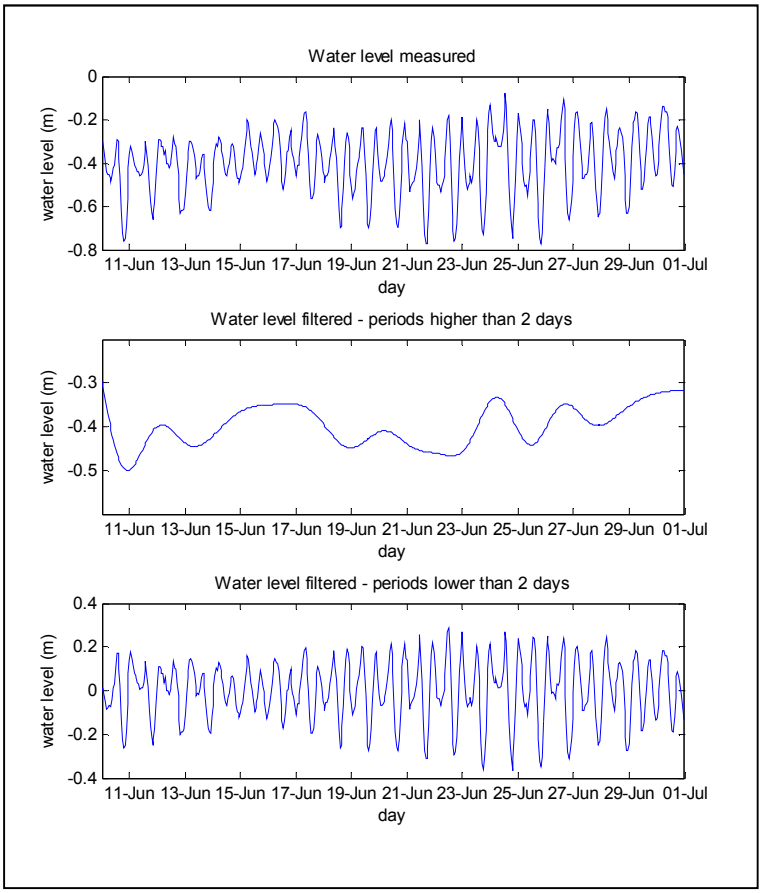

Figure 21 - Filter for Songkhla Water Level Data to be compared with the results. Top: Songkhla Water Level data. Middle: Filtered data (Low frequency) Bottom: Filtered data (High frequency)

As Pattani is located in shallow, protected water, the water level data at this point doesn't completely represent ocean fluctuations. When propagating in bays, like Pattani, tides undergo attenuation. To correct the harmonic amplitudes, Pattani components were multiplied by a factor. This factor varies with frequency because in a bay, semi-diurnal tidal components are preferentially damped compared to diurnal components. This factor was determined by trial and error by comparing the spectral analysis of both

signals until they match (Figure 23). The factor obtained was of 1.1 for diurnal components and 1.5 for semidiurnal components.

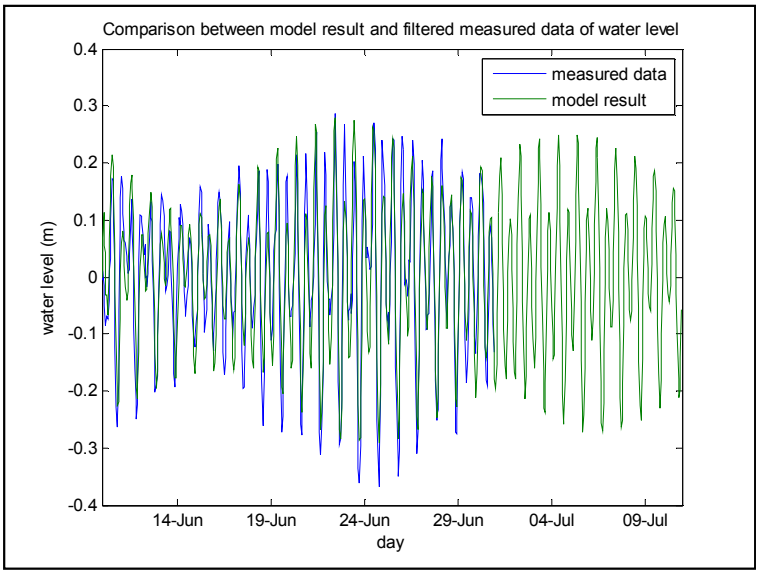

Figure 22 - Comparison between model result and filtered measured data of Songkhla water level during July 1997.

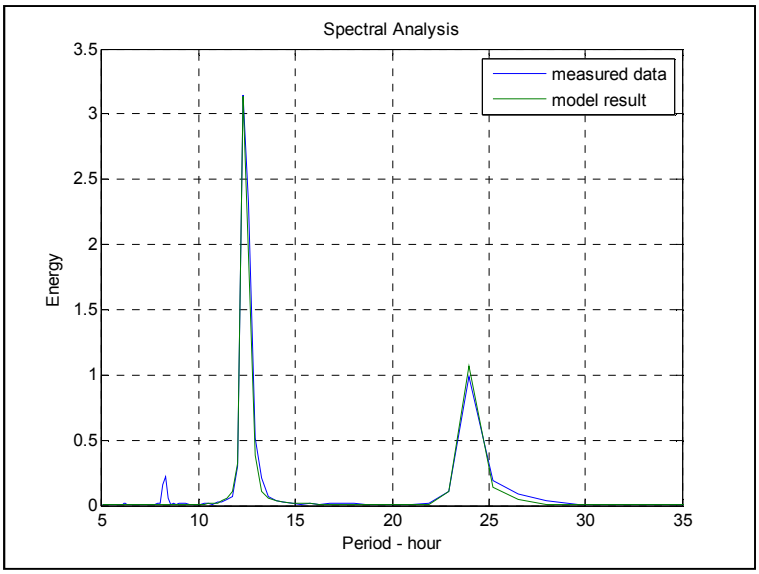

Figure 23 - Spectral Analysis of model result and filtered measured data of Songkhla water level during July 1997

6.4.4 Velocity

Velocity calibration was done using the velocity data at two different locations: North and South of Ko Yo Island. The comparison between the data and model results for the two points are plotted in Figure 24

and Figure 25. The results from North of Koyo show a small phase lag comparing to the data, but the amplitude of the tidal currents are well correlated. The South of Koyo results show smaller amplitude when compared to the data. Despite these small differences, the results were considered good enough.

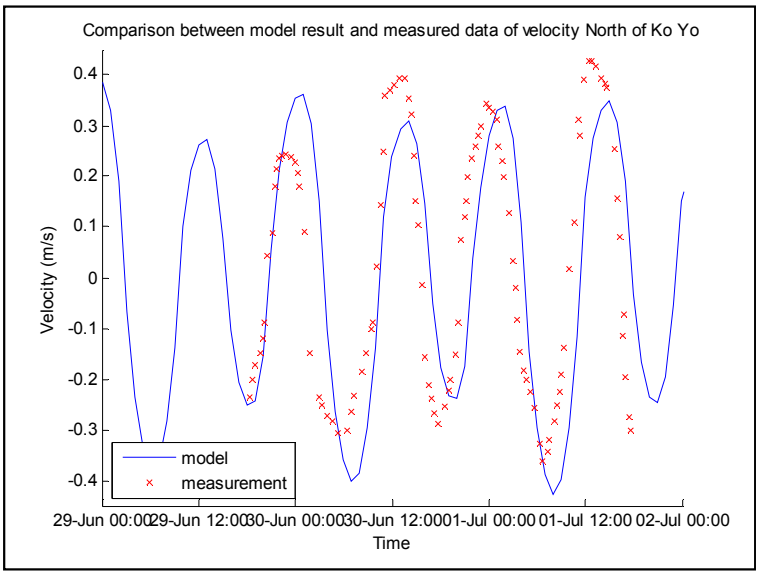

Figure 24 - Comparison between model results and measured data of velocity at North of Ko Yo.

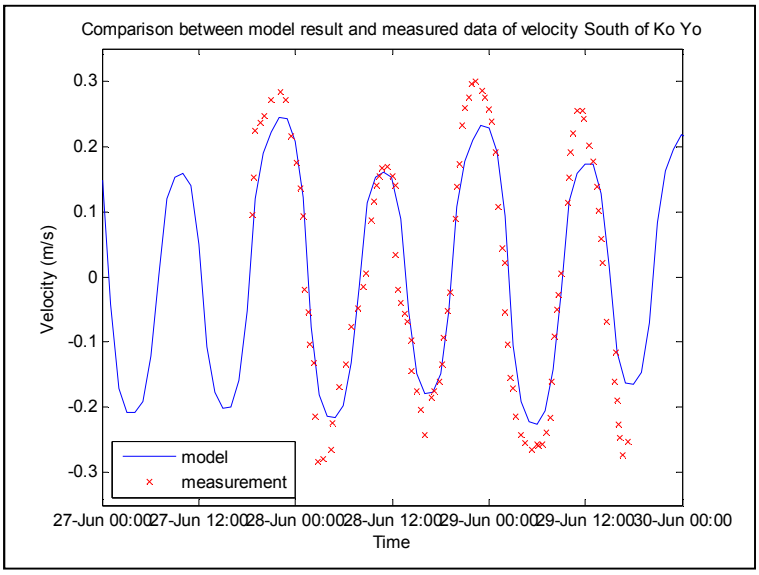

Figure 25 - Comparison between model results and measured data of velocity at South of Ko Yo.

6.4.5 Salinity

The salinity calibration was not straight forward as the velocity and water level. Some issues and doubts appeared while trying to calibrate the model for salinity. The boundary condition of the ocean was set with 35 psu while the two rivers were set with salinity of 0 psu, representing freshwater. The river flows

first were set with the flow given by the two models: GFDL and ECHAM for the 1980-2000 time slice. The results for salinity in point A were a lot fresher than the measurement. Some reasons were pointed for this difference:

- The river flows from the GFDL and ECHAM models don't take into account the deviation of the river for irrigation and human consumption, which can lead to an overestimation.
- The models do not take into account evapotranspiration in the lagoon, which might be very high due to the low latitude of the area and the presence of aquatic plants.
- The measurement point is located in shallow water, which usually is difficult to be modeled.
- The high variability of the natural river flow can also be problem to the modeling. The river flow was considered as the mean flow or October. The natural river flow of the region is dominated by extreme events, which is a characteristic of the monsoon climate. The river has small flow most of the year and during some days, this flow is extremely high. If in this specific year no extreme evens have occurred during or before the measurement period, the real river flow could be much lower than the mean river flow for the considered month.

Taking all these reasons into account, the calibration of the model for salinity was done by reducing the river flows until the measured data and model results match. These values are around 5% of the wet month of ECHAM model and 4% of GFDL (Table 9). The comparison between the model result and the data are plotted in Figure 26.

Table 9 - River flows used to calibrate the model.

River	Flow (m^3/s)
Utaphao	4
Rattaphum	1

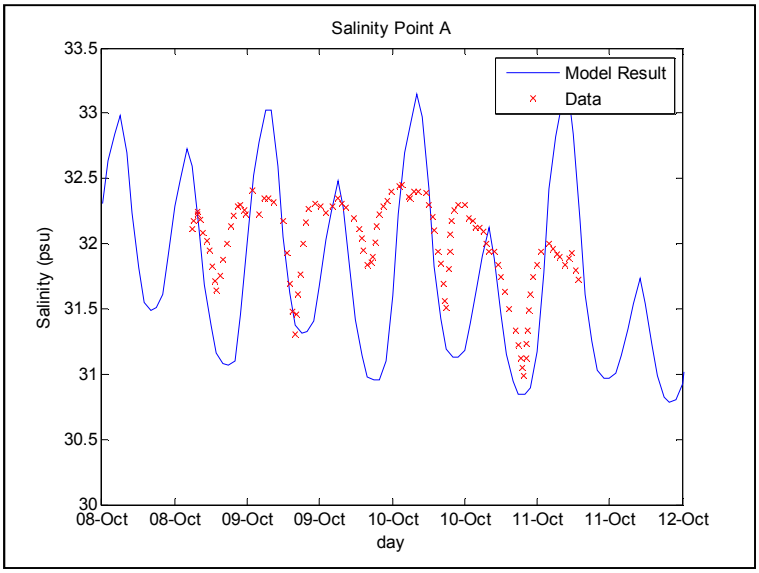

Figure 26 - Comparison between model results and measured data of salitiny at Point A. Riverflow was obtained from ECHAM model output for the 1980-2000 time slice.

7. Simulations

7.1. Scenarios

After the calibration, several scenarios were defined to simulate current and future conditions. For each scenario, a period of 15 days was simulated using Delft3D-Flow and Delft3D-WAQ. The scenarios are summarized in Table 10 and Table 11. To represent the river flows, two models were used: GFDL and ECHAM. These models give the current and future conditions, represented by the year 2000 and 2100 respectively. The dry month is represented by February, while the wet is October. Because the uncertainty about the river flows, two different percentages of the flow given by the two models were used: 5% and 20%.

To represent the sea level rise for the year 2100, the bathymetry for the entire region was deepened by 0.79m, which represents the worst case estimate of IPCC for the year 2100.

Table 10 – Simulated scenarios with 5% of the rivers flows

Model	GFDL				ECHAM			
Year	2000		2100		2000		2100	
Season	wet	dry	wet	dry	wet	dry	wet	dry
Total Flow	5	0.4	4.6	0.065	6.1	0.15	6.7	0.32
Utaphao	4	0.32	3.68	0.052	4.88	0.12	5.36	0.256
Rattaphum	1	0.08	0.92	0.0057	1.22	0.03	1.34	0.064

Table 11 - Simulated scenarios with 20% of the rivers flows

Model	GFDL				ECHAM			
Year	2000		2100		2000		2100	
Season	wet	dry	wet	dry	wet	dry	wet	dry
Total Flow	20	2	18.4	0.26	24.4	0.6	26.8	1.3
Utaphao	16	1.28	14.72	0.208	19.52	0.48	21.44	1.04
Rattaphum	4	0.32	3.68	0.052	4.88	0.12	5.36	0.26

7.2. Circulation pattern

The model has been employed to simulate circulation pattern in Thale Sap Songkhla. All the simulations showed a similar circulation pattern, with different magnitudes. Figure 27 shows the Water level results for the simulation using ECHAM model for October of 2000 (wet season) with the four points characterizing typical current vectors at 3-h intervals starting from the maximum flood current (13th October 2000 at 22:00h).

At the first stage, the lake geometry and bathymetry play a crucial role in controlling circulation with the current prevailing in the deep channel. The maximum current speed of about 1 m/s is in the deep channel of the lake entrance. The flow then diverges into two stream paths passing north and south of Ko Yo (Figure 28).

Three hours later, slack tide is present in the Thale Sap Songkhla. A maximum current speed of around 0.5 m/s is predicted in the channel.

After 6 hours, the flow turning to ebb current. A similar current pattern can be expected as previously shown for the maximum flood. The dominate current prevails in the deep channel and north of Ko Yo. The flow continues ebbing after 9 h and a slack tide occurs throughout the lake.

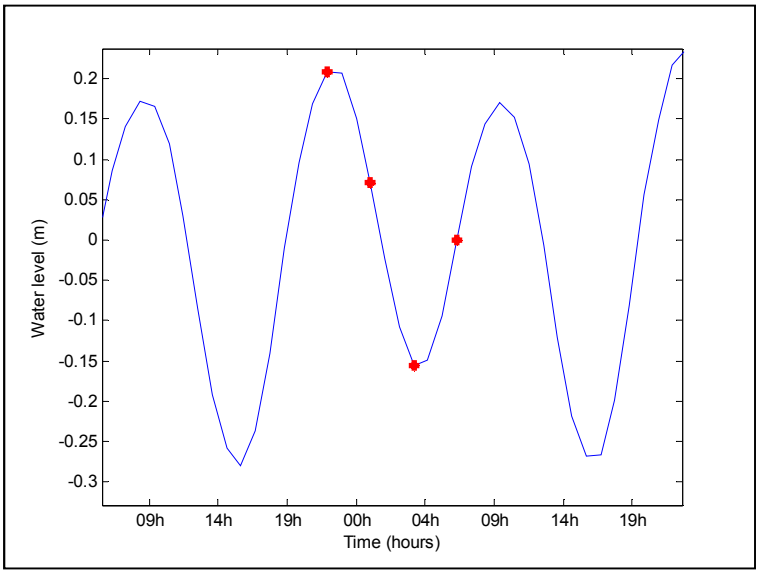

Figure 27 - Water level results for the simulation ECHAM-2000-wet showing the four stages of tides at which circulation patterns were compared

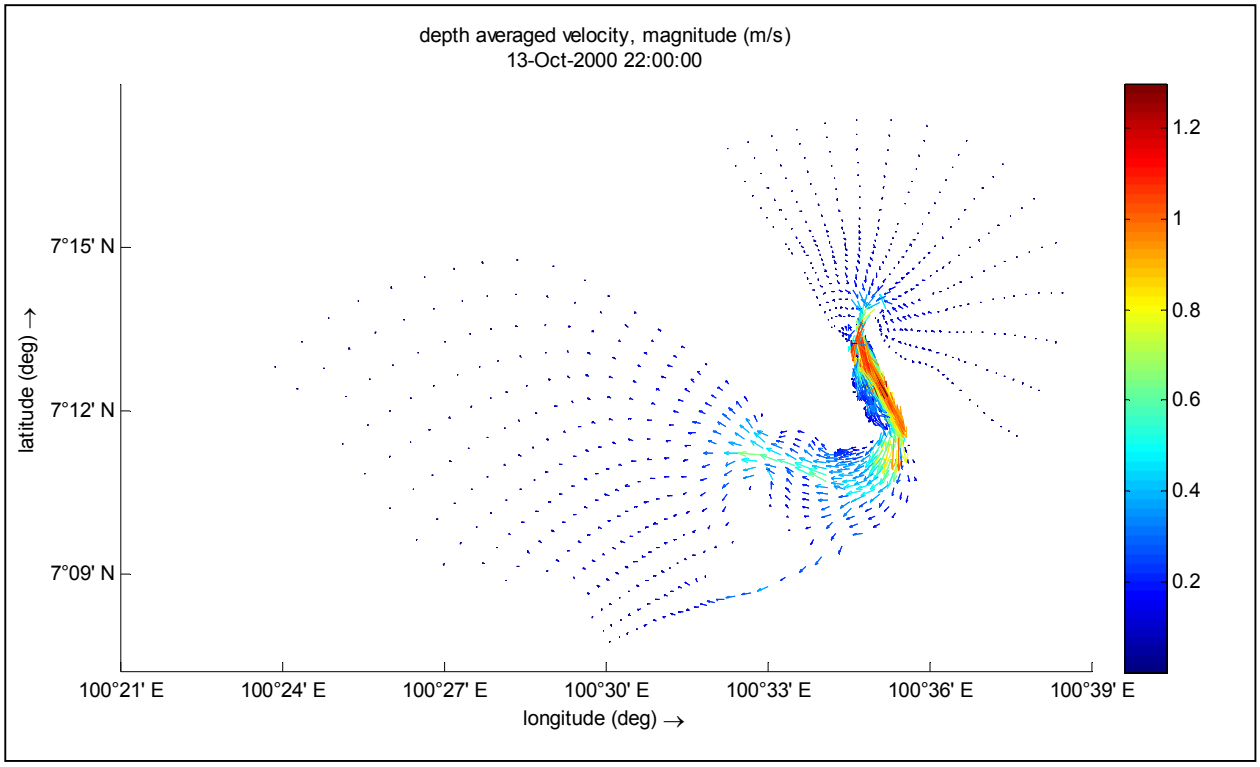
depth averaged velocity, magnitude (m/s)
13-Oct-2000 22:00:00
7°15' N
7°12' N
7°09' N
latitude (deg) →
100°21' E
100°24' E
100°27' E
100°30' E
100°33' E
100°36' E
100°39' E
longitude (deg) →
1.2
1
0.8
0.6
0.4
0.2

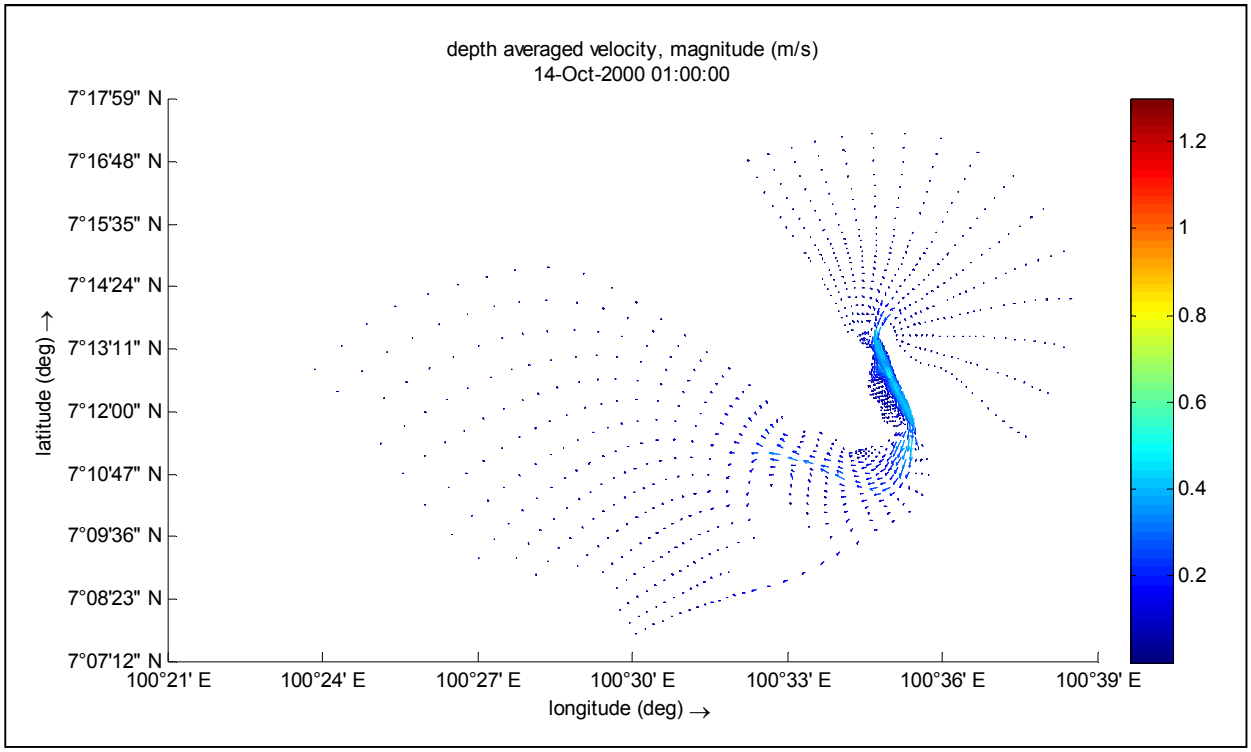
depth averaged velocity, magnitude (m/s)
14-Oct-2000 01:00:00
7°17'59" N
7°16'48" N
7°15'35" N
7°14'24" N
7°13'11" N
7°12'00" N
7°10'47" N
7°09'36" N
7°08'23" N
7°07'12" N
latitude (deg) →
100°21' E
100°24' E
100°27' E
100°30' E
100°33' E
100°36' E
100°39' E
longitude (deg) →
1.2
1
0.8
0.6
0.4
0.2

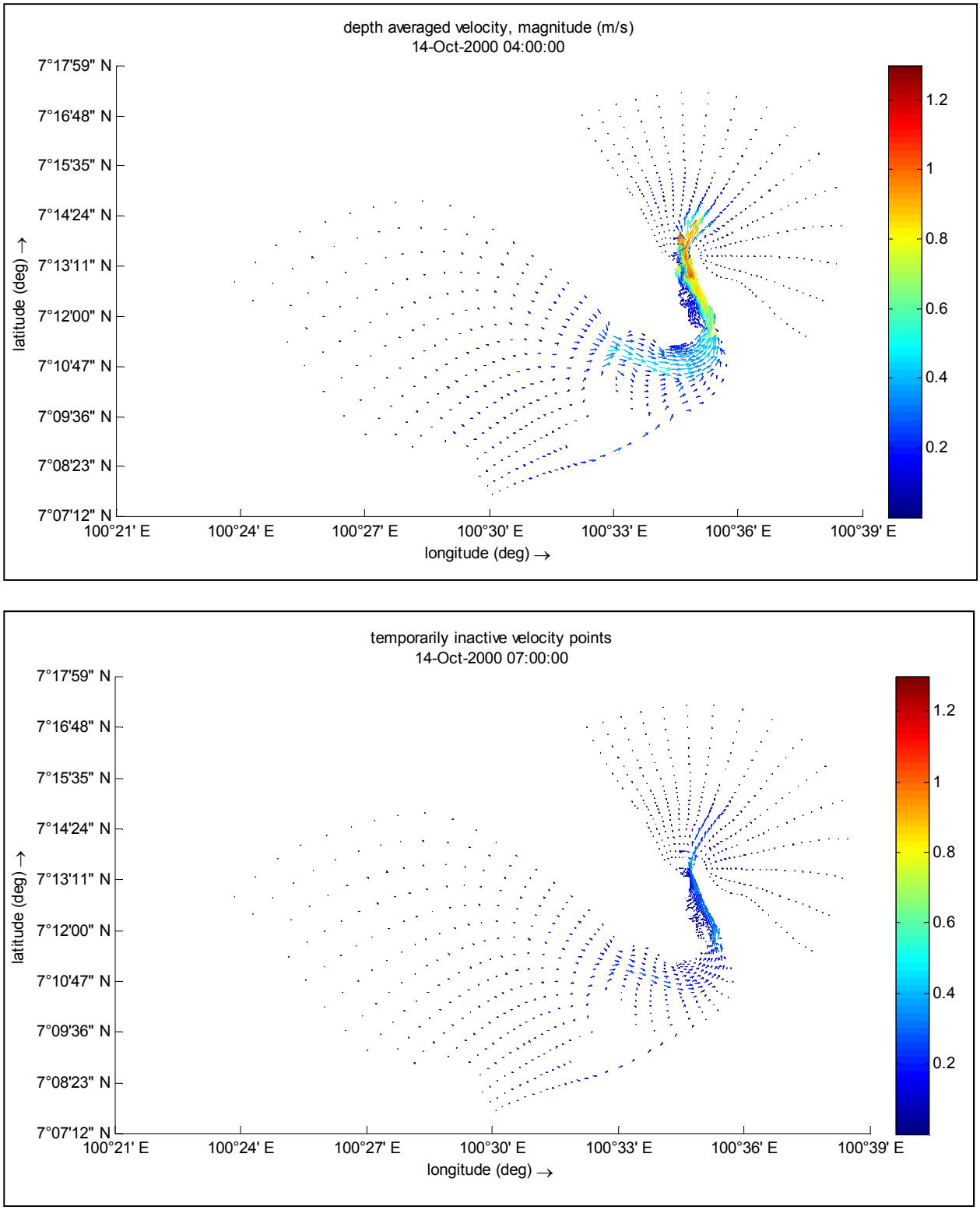

Figure 28 - Circulation pattern in Thale Sap Songkhla for 3 hours interval. Colors indicate speed.

7.3. Velocity

The maximum velocities at the inlet are represented in Table 12 and Table 13 According to the results, there are no significant changes of velocities at the inlet between the dry and wet months or between scenarios with 5% and 20% of river flow, which means that probably the river discharges doesn't have high influence on velocities at the inlet. Comparing the current and future scenarios, it can be observed that the maximum velocities in the future will be higher than today due to sea level rise, this increase corresponds to around 20% for all cases. However, it is likely that the inlet morphology will also change in the future in order to preserve inlet equilibrium velocities of around 1 ms^{-1}.

Table 12 - Maximum velocities at the inlet for the scenarios with 5% of river flow

	GFDL				ECHAM			
	2000		2100		2000		2100	
Season	wet	dry	wet	dry	wet	dry	wet	dry
Maximum velocity (inlet)	1.05	1.02	1.24	1.25	1.06	1.02	1.24	1.25

Table 13 - Maximum velocities at the inlet for the scenarios with 20% of river flow

	GFDL				ECHAM			
	2000		2100		2000		2100	
Season	wet	dry	wet	dry	wet	dry	wet	dry
Maximum velocity (inlet)	1.04	1.03	1.22	1.25	1.06	1.03	1.23	1.25

7.4. Flushing time

To calculate the flushing time, Delft-WAQ model was used. The transport and dispersion of a conservative tracer in the lagoon and its exchange with the ocean is examined. A uniform concentration of 1mg/l is set inside the lagoon, while a concentration of 0mg/l is set as the ocean boundary condition. Hydrodynamic results of simulations with different conditions of river flow and sea level as defined earlier was coupled with this model. The concentrations averaged for the entire lagoon for each time step is calculated to investigate flushing of the lagoon. This signal is filtered to eliminate high frequencies due to tide oscillations and is represented in Figure 29 (5% of river flow) and Figure 30 (20% of river flow).

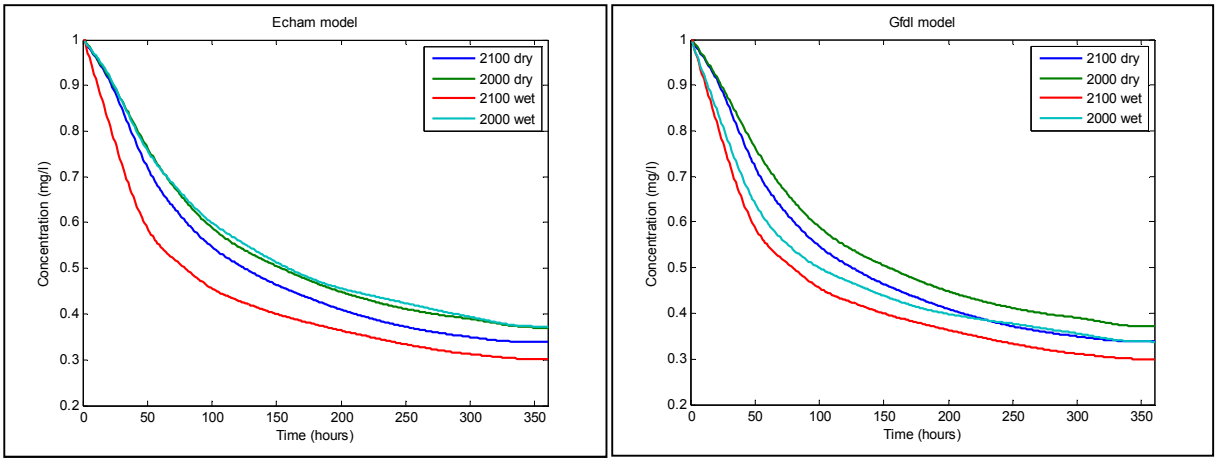

Figure 29 – Filtered Mean results of concentration for the entire lagoon of a tracer given by Delft3D with 5% riverflows derived from GFDL (left) and ECHAM (right) models.

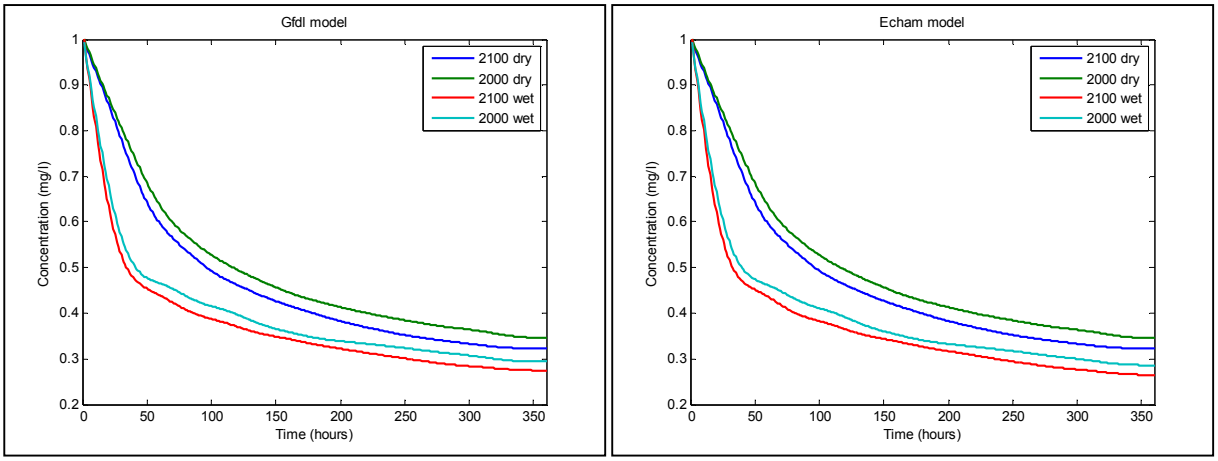

Figure 30 - Filtered Mean results of concentration for the entire lagoon of a tracer given by Delft3D with 20% riverflows derived from GFDL (left) and ECHAM (right) models.

The percentage of the initial mass of the tracer remaining within the lagoon was calculated at each time step and was expressed as an exponential curve of the following form to obtain the e-folding time (the time taken for the initial mass to reduce to 1/e of initial mass) for the lagoon.

$$Y = Aexp(bT)$$

Where,

Y = Percentage mass remaining,

T = Time in hours,

A, b = constants

The e-folding time is an estimate the flushing time of the lagoon (Aubrey et. al., 1993). The results are summarized in Table 14 and Table 15. The results show that for all cases, the flushing time for wet months is smaller than for dry months. Scenarios with 20% of river flow also showed smaller flushing times comparing with the 5% ones. The rivers help to flush the lagoon so its flow is inversely proportional to flushing time. Also, the flushing time will decrease in future scenarios of sea level rise; this decrease will be different, depending on the river flow changes. When the river flow increase, which is the case of ECHAM model, the flushing time have a higher decrease.

Table 14 - Calculated flushing time for the scenarios with 5% of river flow

	GFDL				ECHAM			
	2000		2100		2000		2100	
Season	wet	dry	wet	dry	wet	dry	wet	dry
Flusing time (h)	270.05	319.15	199.87	267.36	318.92	331.02	200.70	267.38

Table 15 - Calculated flushing time for the scenarios with 20% of river flow

	GFDL				ECHAM			
	2000		2100		2000		2100	
Season	wet	dry	wet	dry	wet	dry	wet	dry
Flusing time (h)	146.6	281.8	110.4	235.9	134.5	281.2	102.7	236.1

7.5. Salinity

All the simulations showed a similar salinity distribution, with different magnitudes. Figure 31 shows the result of depth average salinity of the entire lagoon for the scenarios using ECHAM model for the instant 13th October 2000 at 22:00h. This result shows a salinity of 35 psu outside the lagoon. Inside the lagoon the salinity decreases near the rivers, with a minimum of 25 psu close to the river mouth.

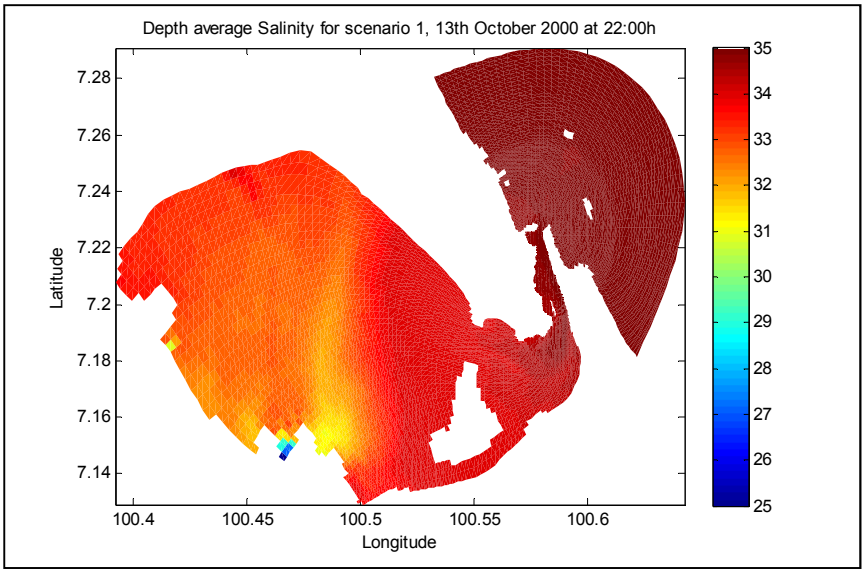

Figure 31 – Result for depth average salinity for Scenario ECHAM - 2000 - wet for the instant 13th October 2000 at 22:00h

There is variation of salinity in the lagoon due to tides; Figure 32 represents this variation for a point in the center of the lagoon for one scenario. This point was chosen because is a point influenced by tides and river flows. It can be seen that, after stabilization, the mean salinity at this point is about 33 psu with amplitude of 1.5 psu.

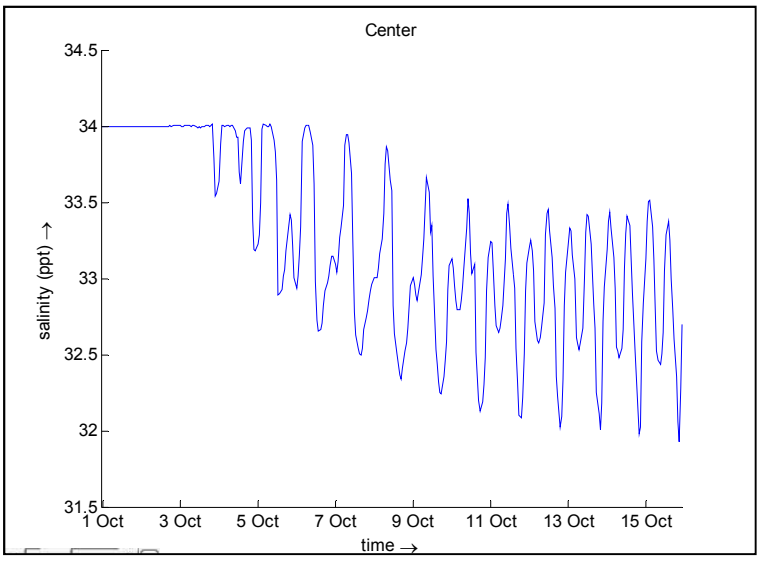

Figure 32 - Salinity results for a point in the center of lagoon for Scenario ECHAM – 2000 – wet

The mean salinity for a point in the center of the lagoon was calculated and the results are summarized in Table 16 and Table 17. During wet months, the salinity will increase for future scenarios, especially

considering the simulations with 20% of river flow. For both models, the results showed a difference in salinities between wet and dry months. The wet months presents lower salinity than the dry months for all the simulations, but especially for the scenarios with 20% of river flow, where the difference can reach more than 15 psu. The salinity during the dry months didn't show much change for all the scenarios. However, it should be noted that CC driven variation in temperature and hence evaporation was not considered in these simulations.

Table 16 - Mean salinity at a point in center of the lagoon for the different scenarios with 5% river flow

	GFDL				ECHAM			
	2000		2100		2000		2100	
Season	wet	dry	wet	dry	wet	dry	wet	dry
Salinity (psu)	31.52	34	31.44	34	33.24	34	31.13	34

Table 17 - Mean salinity at a point in center of the lagoon for the different scenarios with 20% river flow

	GFDL				ECHAM			
	2000		2100		2000		2100	
Season	wet	dry	wet	dry	wet	dry	wet	dry
Salinity (psu)	15.8	33.0	17.14	33.0	13.05	33.0	14.3	32.9

7.6. Stratification

The stratification of the lagoon is defined as the difference between the bottom and the top layers of the simulation results. Figure 33 shows this difference for the entire lagoon for the scenarios when using riverflow derived from the ECHAM model for the instant 13th October 2000 at 22:00h. It can be observed that there is no stratification in the east part of the lagoon. The greatest stratification is found on the western part, especially close to the river mouths, where it can reaches 15 psu.

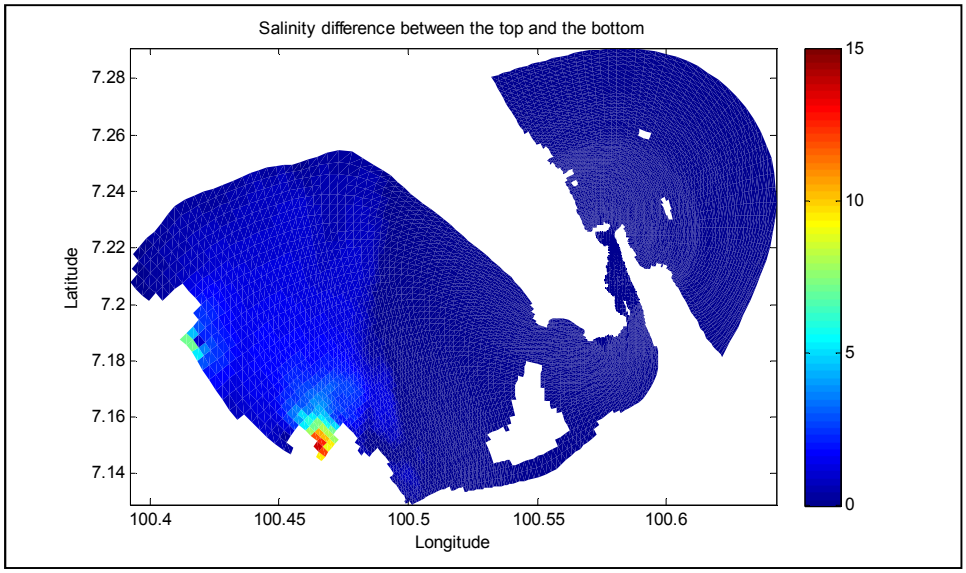

Figure 33- Difference between the bottom and the top layer of salinity results for Scenario ECHAM - 2000 - wet for the instant 13th October 2000 at 22:00h

Stratification also varies with tide; Figure 34 represents this variation for one scenario: Wet season of 2000 with riverflow derived from the ECHAM model for a point in the west part of the lagoon. It can be seen that, after stabilization, the stratification reaches a mean of 1.4psu with amplitude of 0.4psu.

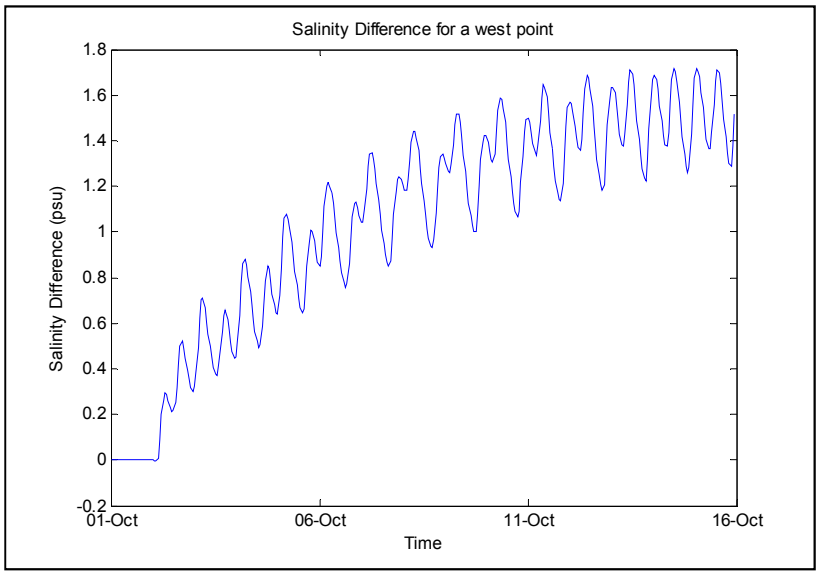

Figure 34- Difference between the bottom and the top layer of salinity results for a point in the west of lagoon for Scenario ECHAM – 2000 – wet

The maximum stratification for a point located in the west part of the lagoon was calculated and the results are summarized in Table 18 and Table 19. This point was chosen because is a point with significant stratification and not very close to the rivers. The results show that the stratification for this point is greater during wet season. Comparing current with future scenarios, it can be observed that during

wet months there is a decrease of stratification in the future for the simulations with 5% of river flow and a increase of stratification for simulations with 20% of river flow. For the dry months, all simulations showed an increase in stratification in future. It should be noted that CC driven variations in future wind effects were not considered in these simulations.

Table 18 – Average Difference salinity at a point in the western part of the lagoon for the different scenarios with 5% of river flow

	GFDL				ECHAM			
	2000		2100		2000		2100	
Season	wet	dry	wet	dry	wet	dry	wet	dry
Difference (psu)	1.45	0.33	1.09	0.83	1.72	0.29	1.27	0.81

Table 19 - Average Difference salinity at a point in the western part of the lagoon for the different scenarios with 20% of river flow

	GFDL				ECHAM			
	2000		2100		2000		2100	
Season	wet	dry	wet	dry	wet	dry	wet	dry
Difference (psu)	2.17	0.73	2.30	0.82	2.15	0.36	2.92	0.68

8. Conclusions and Recommendations

The available data of water level, velocity, salinity and streamflow of Songkhla Lagoon were analyzed and some conclusions were reached.

Spectral analysis of water level data showed three main periods of oscillation: annual, semidiurnal and diurnal. The annual signal is related to the monsoon climate of the region, with high water level during the wet season from November to January and low water level during the dry season, from June to August.

The semidiurnal and diurnal periods are related to tides. Delft Dashboard was not successful to represent the tides in the region. T-tides and World tides, two Matlab routines, presented similar results for tidal harmonic components, however, World tides presented slightly better results and was adopted in this study. The results showed that semi-diurnal tidal components were preferentially damped compared to diurnal components, the damping factor was 1.1 and 1.5 for diurnal and semidiurnal amplitudes respectively. The phases presented a shift between the World tides and Delft3D.

The riverflows obtained using dynamically downscaled projections from two global models GFDL and ECHAM showed different results. The year of 2000, both showed the same behavior, but different magnitudes. For the year 2100 they showed opposite behavior, ECHAM predicts an increase of river flow, while GFDL predicts a decrease. The high variability associated to the river flow and uncertainties of long prediction are possible reasons for this difference.

Delft 3D model was used to simulate the hydrodynamic conditions of Songkhla lagoon in Thailand and proved to be an efficient model for this purpose. The optimum time step for the chosen grid was 30 second. The appropriate eddy viscosity found was $0.1 m^2/s$ and eddy diffusivity of $0.05 m^2/s$.

The calibration for water level and velocity showed good correlation. The calibration for salinity was achieve with a river flow of about 5% of the given by the world models. Some hypotheses for this include: fresh water deviation for irrigation and human consumption; evapotranspiration of the lagoon; the inappropriate position of the measured data; and a high variability of the river flow.

Some scenarios were created to simulate current and future scenarios for the region during dry and wet seasons and for river flow of 5% and 20% of the two available models, with a total of 16 simulations. The results show that circulation in Thale Sap Songkhla is strongly influenced by the lake geometry. The strong flow, coming from the lake entrance, deflects to the north and the south of Ko Yo. The velocities at

the entrance channel are around 1m/s and the simulations show an increase of 20% for the year 2100 (in the absence of morphological adjustments, which were not simulated here).

The flushing time is smaller during wet months, because of the higher river flows and is expected to decrease for future scenarios due to the sea level rise.

Salinity also presented different values for wet and dry months, being higher during dry months because the weaker river flows. Stratification results showed a higher stratification during wet season. The results suggest distinct behavior for future scenarios, during wet months the stratification can decrease or increase depending on river flow considerations and during dry months, it will increase for future scenarios. This result was not sufficient and further analysis should be done to find the reasons for this behavior.

The main limitation of this study is the lack of data for the region. Due to this limitation, the results of this study should be interpreted in a qualitative way. The comparison between the scenarios are valid, but the absolute values needs further investigation.

For future modeling efforts, there is an urgent need for high quality simultaneous measurements of water level, velocity, and salinity at several points spread across the lagoon over a duration of at least 30 days during both the wet and dry seasons. River discharge data and atmospheric data, such as: wind, evaporation, rainfall, solar incidence should also be measured.

Preferable these measurements should be repeated over a few years to take into account annual variations. Sufficient model validation will be impossible without such high quality, consistent data, which will inevitably result in unreliable predictions

A more complete study of future scenarios of river flow discharge for this region using global models should also be performed to understand the impacts of climate change not only for the lagoon but for the entire region.

The vertical resolution for future models should be increased and to perform a more precise investigation other variables should be include, such as: evapotranspiration of the lagoon; storms surges; and winds.

9. References

Anthony, A., J. Atwood, P. August, C. Byron, S. Cobb, C. Foster, C. Fry, A. Gold, K. Hagos, L. Heffner, D. Q. Kellogg, K. Lellis-Dibble, J. J. Opaluch, C. Oviatt, A. Pfeiffer-Herbert, N. Rohr, L. Smith, T. Smythe, J. Swift, and N. Vinhateiro. 2009. Coastal lagoons and climate change: ecological and social ramifications in U.S. Atlantic and Gulf coast ecosystems. Ecology and Society 14(1): 8.

Aubrey, D. G.; McSherry, T. R., and Eliet, P.P., 1993. Effects of multiple inlet morphology on tidal exchange: Waquoit Bay, Massachussettes. In: Aubrey, D. G. and Giese, G. S. (eds.), Formation and Evolution of Multiple Tidal Inlets. Washington, D.C., American Geophysical Union, pp. 231-235.

Barnes, H. (1980) Coastal lagoons, Cambridge University Press. 106pp.

Ganasut, J. 2004 Sediment transport and morphological modeling of Songkhla Lagoon, Thailand. Dissertation. Asian Institute of Technology. School of Civil Engineering. Thailand.

Ganasut, J., Weesakul, S., Vongvisessomjai, S. 2005 Hydrodynamic Modeling of Songkhla Lagoon, Thailand. Thammasat Int. J. Sc. Tech., Vol. 10, No. 1.

Haines, P. (2008) Anticipated Response of Coastal Lagoons to Sea Level Rise. IPWEA National Conference August 2008

Kjerfve, B., 1986. Comparative oceanography of of coastal lagoons. In: WOLFE, D.A. (ed.). Estuarine Variability. Academic Press, New York, pp. 63-81.

Kjerfve, B. and Magill, K.E., 1989. Geographic and hydrodynamic characteristics of shallow coastal lagoons. Marine Geology, 88, 187-199

Kjerfve (1994). Kjerfve, B., 1994. Coastal Lagoon Processes. Elsevier Science Publishers, Amsterdam, xx + 577pp.

Miller, J.M.; Pietrafesa, L.J.; Smith, N.P. Principles of hydraulic management of coastal lagoons for aquaculture and fisheries. FAO Fisheries Technical Paper. No. 314. Rome, FAO. 1990. 88p.

Nichols, M.M., and Allen, G., 1981. Sedimentary processes in coastal lagoons. In: Coastal lagoon research, present and future. UNESCO, Paris. Pp. 77-187

Pawlowicz, R. Beardsley, B. and Lentz, S. "Classical tidal harmonic analysis including error estimates in MATLAB using T_TIDE", Computers and Geosciences 28 (2002), 929-937.

Pornpinatepong, K.; Kiripat, S.; Treewanchai, S.; Chongwilaikasaem, S.; Pornsawang, C.; Chantarasap, P.; Chandee, C.; Jantrakul, P. Pollution and Sustainable Fisheries Management in Southern Songkhla Lake, Thailand. 4th World Congress of Environmental and Resource Economists, Montreal, Canada, 2010

Pornpinatepong, S.; Tanaka, H.; Takasaki, M. Application of 2-D Vertically Averaged Boundary-Fitted Coordinate Model of Tidal Circulation in Thale Sap Songkhla, Thailand. Walailak J Sci & Tech 2006 3(1): 105-118

Ranasinghe, R. and Pattiaratchi, C. 1999 Circulation and mixing characteristics of a seasonally open tidal inlet: a field study. Mar. Freshwater Res., 50, 281-90

Sae-Chew, W. Studying waste load dispersion in Songkhla Lake using a simulation model. Climate Variability and Change – Hydrological Impacts (Proceedings of the Fifth FRIEND World Conference held in Havanas, Cuba, November 2006), IAHS Publ. 308, 2006

Smith, NP., 1994. Water, salt and heat balances of coastal lagoons. In Kjerfve, B. (Ed.). Coastal Lagoon processes. Amsterdam, The Netherlands: Elsevier. Elsevier Oceanography Series., vol. 60, p. 69-102.

Viet, N. T., Tanaka, H., Takasaki, M. and Yamaji, H. 2007 In-situ investigation and simulation of water quality changes in Songkhla Lake, Thailand. Proceedings of the 4th Asian and Pacific Coasts Vol. 4., Nanjing, China.

Vongvisessomjai, S. 1999 EIA of salinity barrier construction at Songkhla lagoon, Songklanakarin J. Sci. Technol., 21(4) : 447-471